Earth and Space Science

RESEARCH ARTICLE
10.1029/2024EA003910

Trends of Summer Lake Surface Water Temperature on the Tibetan Plateau and Their Response to Climate Change

Yi Shi[1], Anning Huang[1,2], Yang Wu[3], Lazhu[4], and Lijuan Wen[5]

[1]School of Atmospheric Sciences, Nanjing University, Nanjing, China, [2]Qinghai Lake Comprehensive Observation Research Station, Chinese Academy of Sciences, Gangcha, China, [3]CMA Key Laboratory of Transportation Meteorology, Nanjing Joint Institute for Atmospheric Sciences, Nanjing, China, [4]College of Science, Tibet University, Lhasa, China, [5]Key Laboratory of Land Surface Process and Climate Change in Cold and Arid Regions, Chinese Academy of Sciences, Lanzhou, China

Abstract The Tibetan Plateau (TP) is covered by numerous lakes, and lake surface water temperature (LSWT) is an essential indicator of climate change, while few observations hinder our understanding of LSWT variation and its causes over TP. This study aims to simulate the summer LSWT long-term trends of 81 TP lakes during 1980–2018 and quantify the impacts and contributions of atmospheric variables. Results show that TP lakes warmed with 0.32°C decade^{-1} on average. Northern TP lakes warmed faster than the southern ones (0.44 vs. 0.16°C decade^{-1}) due to stronger trends of atmospheric variables and higher sensitive of colder lakes to atmospheric changes. 55 (67.9%) lakes of the total lakes studied in current work warmed slower than air due to weakened shortwave radiation ($SW_{\downarrow}$). Attribution analysis suggests that the air warming and wetting over TP dominate lakes' warming. Regarding synthesis contributions, air warming contributed 79.3%, with increased surface air temperature (SAT) and downward longwave radiation ($LW_{\downarrow}$) accounting for 41.6% and 37.7%, respectively, and air wetting indicated by increased surface specific humidity (SSH) contributed 39.0%, followed by a positive contribution (16.8%) from declined wind speed (WS). The negative contribution (−35.1%) from weakened $SW_{\downarrow}$ nearly counterbalances the positive effects of increased $LW_{\downarrow}$. 55.1% of the total synthesis contribution arises from the cross contribution through interactions among atmospheric variables and is mainly reflected in SAT and SSH, accounting for 26.8% and 24.8%, respectively. The findings enhance understanding of climate change impacts on lake systems and offer insights for lake resource management.

Plain Language Summary Lake surface water temperature (LSWT) has been rising in recent decades in response to climate change on both regional and global scales, yet a geographical map of LSWT variation and quantitative attribution over Tibetan Plateau (TP) are not well presented due to inadequate observations. Here, we analyze the summer LSWT trends of 81 large TP lakes, each with an area exceeding 50 km^2, based on one-dimensional lake model simulations during 1978–2018. The results suggest a mean warming rate of 0.32°C decade^{-1} for all the studied lakes, with faster lake warming in colder regions. The main cause for LSWT increase over TP is the air warming and wetting. Specifically, the main positive contributors are the increased air temperature, longwave radiation, and moisture, while the decreased wind speed makes a secondary contribution. The negative contributor is the decreased solar radiation, which essentially offsets the positive effects of increased longwave radiation, leading to a smaller increase of LSWT than the ambient air temperature.

Key Points:

- Lakes on Tibetan Plateau (TP) warmed by 0.32°C decade^{-1} during the summers of 1980–2018, due to the air warming and wetting
- Most ice-covered lakes warm slower than the ambient air due to weakened shortwave radiation over TP
- Colder lakes are more sensitive to atmospheric changes than warmer lakes

Supporting Information:

Supporting Information may be found in the online version of this article.

Correspondence to:

A. Huang and Y. Wu,
anhuang@nju.edu.cn;
wuy@cma.gov.cn

Citation:

Shi, Y., Huang, A., Wu, Y., Lazhu, & Wen, L. (2024). Trends of summer lake surface water temperature on the Tibetan plateau and their response to climate change. *Earth and Space Science*, *11*, e2024EA003910. https://doi.org/10.1029/2024EA003910

Received 17 AUG 2024
Accepted 30 NOV 2024

Author Contributions:

Conceptualization: Anning Huang
Data curation: Yi Shi, Yang Wu, Lijuan Wen
Formal analysis: Anning Huang, Lazhu, Lijuan Wen
Investigation: Yang Wu, Lazhu
Methodology: Yi Shi, Yang Wu
Resources: Yi Shi, Yang Wu, Lazhu, Lijuan Wen
Software: Yi Shi, Yang Wu
Supervision: Anning Huang
Validation: Yi Shi, Anning Huang, Lijuan Wen
Visualization: Yi Shi
Writing – original draft: Yi Shi, Anning Huang, Yang Wu
Writing – review & editing: Yi Shi, Anning Huang, Yang Wu, Lazhu, Lijuan Wen

1. Introduction

Lakes are the nexus of interactions among different spheres of the Earth's surface system and are therefore sensitive to climate change (Adrian et al., 2009). As a critical indicator of lake and climate change, lake surface water temperature (LSWT) has exhibited a noticeable increase globally (Adrian et al., 2009; Woolway et al., 2020), with an average increasing rate of 0.34°C decade^{-1} during the summers of 1985–2009 (O'Reilly et al., 2015). Physically, rising LSWT can intensify the thermal stratification (Anderson et al., 2021; Kraemer et al., 2015) and then shift the mixing regimes (Woolway et al., 2019; Wu et al., 2024). Lakes warming is considered caused by climate changes, such as air warming (Piccolroaz et al., 2013; Schneider & Hook, 2010), solar brightening (Fink et al., 2014; Schmid & Köster, 2016), and wind stilling (Huang et al., 2012; Woolway et al., 2019). Therefore, a reasonable prediction for changes in the lake system requires an integrated understanding of the LSWT response to atmospheric variables.

Known as the "water tower of Asia" (Qiu, 2008; Xu et al., 2008), TP is home to more than 1400 lakes with an area exceeding 1 km^2 (Zhang et al., 2019), most of which are saltwater and ice-covered with an average elevation over 4,000 m (Cai et al., 2019; C. Liu et al., 2021). In the studies of Cai et al. (2019), the ice cover duration of TP lakes with elevation >2,800 m ranges from 87 to 241 days with an average of about 158 days, with ice-on occurring from October to January and ice-off from March to July. However, TP lakes are frequently omitted from global-scale analyses about LSWT on a global scale (Schmid et al., 2014; Woolway & Merchant, 2017) because of the unique geological environment and alpine climate (Kuang & Jiao, 2016). Hence, investigating TP lakes' response to climate change is of exceptional significance.

TP has experienced distinctive climate shifts since the 1980s, including surface air warming, moistening, solar dimming, and wind stilling (Kuang & Jiao, 2016; Yang et al., 2014), where solar dimming presents a unique aspect of TP climate change, contrasting with the other regions especially Europe (Schmid & Köster, 2016; Yuan et al., 2021). Under the climate changes, the warming trends of TP lakes were revealed based on satellite observations (Liu et al., 2019; Wan et al., 2018; Zhang et al., 2014) and numerical models (Guo et al., 2022) on different time scales. Some studies focus on several large lakes and qualitatively investigate the effects of TP climate changes on lake warming.

In these case studies, besides enhanced air temperature and longwave radiation (Huang et al., 2017), reduced wind speed (Su et al., 2019) and increased specific humidity (Shi et al., 2022) were also identified as contributors to warming in large lakes. Besides, these studies consistently indicated that weakened shortwave radiation over lakes is associated with a slower warming rate compared to the air. In the case of Lake Ngoring and Lake Gyaring on TP, decreased solar radiation even counteracted the contribution of rising air temperature and humidity, resulting in no significant trend in LSWT (Kirillin et al., 2017). In contrast, other seasonal ice-covered lakes globally exhibit more rapid warming than air due to the synergy of increasing air temperature and shortwave radiation (O'Reilly et al., 2015). These reports introduce the hypothesis that the majority of lakes on the TP warm at a slower rate than the air for the attenuation of shortwave radiation.

Nevertheless, few studies analyzed the quantitative contribution of climate change on LSWT variation over the whole Tibetan Plateau, and most of the studies focused on several large lakes. In this study, we focus on the TP region, which has many seasonally ice-covered lakes and is undergoing complex climate changes, and select 81 lakes, each with an area ≥50 km^2, to achieve the following objectives: (a) To analyze the spatial pattern of LSWT trends during 1980–2018. Here the one-dimensional lake numerical model WRF-Lake is an effective instrument for reproducing long-term historical LSWT variations and trends, and the results will be validated with the Moderate Resolution Imaging Spectroradiometer (MODIS) Land Surface Temperature (i.e., the Earth's surface temperature) data. (b) To quantify the contributions of atmospheric forcings to LSWT trend, especially to verify the hypothesis that solar dimming would slow down TP lakes warming. For this purpose, we apply an integrated analytical approach based on the numerical sensitivity experiments and partial derivative decomposition method (Shi et al., 2022). Compared to the traditional method that quantifies contributions by taking the difference in simulated LSWT trends before and after de-trending the target atmospheric forcing variable one-by-one (Huang et al., 2023; Li et al., 2019, 2023), this method not only calculates the contribution of each variable but also decomposes the contribution into independent and cross parts, thereby eliminating the confounding effects from intrinsic collinearity among atmospheric variables. The main findings of this study may provide valuable insights for understanding and predicting the LWST changes over TP.

2. Material and Methods

2.1. Study Area

With an average elevation of over 4,000 m, TP presents a typical alpine climate characterized by low temperatures, high solar radiation, and large daily and small annual air temperature differences. Regionally, the summer climate is warmer and wetter in the southeast than in the northwest, influenced by the South Asian and East Asian monsoons (Kuang & Jiao, 2016). Figure 1 shows the geographic location of selected 81 large lakes over TP. The selected lakes range 30.70–38.86°E in latitude, 79.78–100.20°E in longitude, 2,795–5,158 m in elevation, 53.10–4,226.24 km^2 in surface area, 1.2–120.0 m in mean depth. Information on all 81 lakes is listed in Table S1 of Supporting Information S1. Notably, most meteorological stations are located in eastern and southern TP with more suitable climates, while most lakes are in the central and western TP, lacking in situ observations.

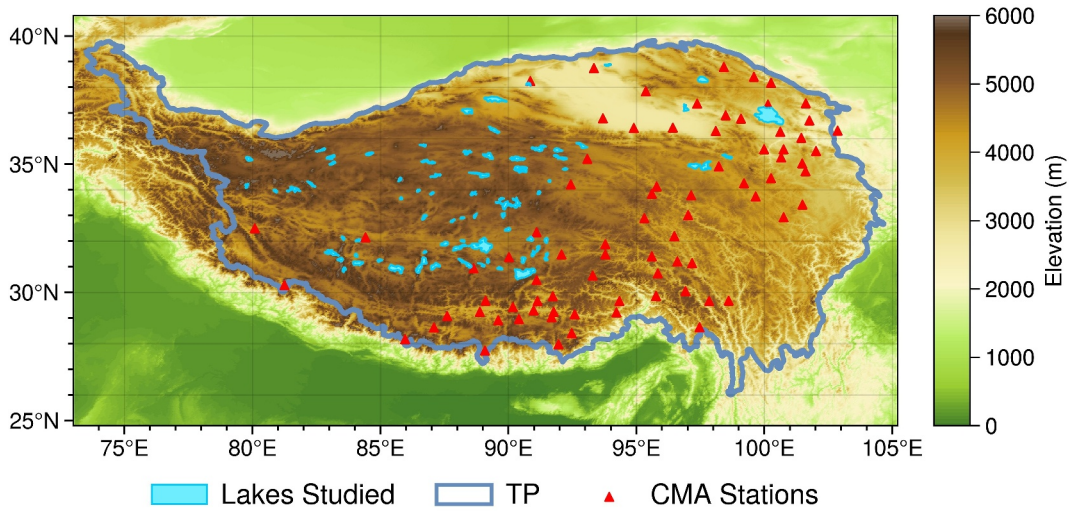

Figure 1. Spatial distribution of land topography and studied lakes (light blue colored areas) over TP. The red triangles represent the China Meteorological Administration (CMA) stations, and the blue line outlines TP.

2.2. Data Set and Processing

2.2.1. Geographical and Physical Data of Lakes

In this study, we obtain the latitude, longitude, elevation, and mean depth for each selected lake from Wang et al. (2021), and the salinity of most lakes from the in situ water quality investigation of TP lakes (C. Liu et al., 2021). The light extinction coefficient (η, in m^{-1}) is a crucial lake-specific property determining the distribution of downward solar radiation at different lake depths. For parameter optimization later, we estimate an initial η_0 for each lake by using the satellite-retrieved Secchi depth (SD, in m; Tao et al., 2022) according to the empirical formula Equation 1 (Bukata et al., 1988):

$$\eta_0 = \begin{cases} \dfrac{0.757}{SD} + 0.07, & 2 \le \mathrm{SD} \le 10 \\ \dfrac{1.7}{SD}, & \mathrm{SD} < 2 \text{ or } \mathrm{SD} > 10 \end{cases} \quad (1)$$

2.2.2. Atmospheric Forcing Data and Elevation Correction

The Japanese 55-year Reanalysis (JRA-55) data set (Harada et al., 2016; Kobayashi et al., 2015) during 1979–2018, whose applicability has been verified in TP area (Xu et al., 2021; Yao & Li, 2016) and widely used in studying the TP climate change (Chen et al., 2019; Zhang et al., 2021), is utilized to drive WRF-Lake model (see Section 2.3). The selected JRA-55 variables include surface air temperature (SAT), surface pressure (SP), surface specific humidity (SSH), relative humidity (RH), surface wind speed (WS), and surface downward shortwave ($SW_{\downarrow}$) and longwave radiation ($LW_{\downarrow}$), where SAT, SP, SSH, RH, WS are 6-hr surface analysis fields and $SW_{\downarrow}$, $LW_{\downarrow}$ are 3-hr average diagnostic fields. The TL319L60 model grid was converted to a regular latitude-longitude Gaussian grid (nominally 0.5625°) while downloading from NCAR.

Generally, the surface wind speed is stronger over the lake than over adjacent land due to the lower roughness of the water surface. However, since the JRA-55 grids cannot distinguish most lakes, the above wind speed (WS) is expected to be smaller than the actual over-lake wind speed (WS_{Lake}). Hence, an empirical wind scaling formula Equation 2 suggested by Hsu (1988), which has been widely used for wind speed correction in lake simulations (Huang et al., 2021; Layden et al., 2016), is used to obtain WS_{Lake}:

$$\mathrm{WS}_{\mathrm{Lake}} = 1.17\mathrm{WS} + 1.62 \quad (2)$$

Then, for each studied lake, we select the JRA-55 data within the lake boundary and average it to yield the time series of atmospheric forcing variables. However, as the mean elevation for the selected JRA-55 grids (Z, in m) differs from the actual lake elevation (Z_L, in m), elevation adjustment is essential to correct the thermodynamic variables in JRA-55 atmospheric forcing. The corrected surface air pressure (SP', in hPa) and temperature (SAT', in K) are formulated as Hafner and Smith (1985):

$$\mathrm{SP}' = \mathrm{SP}\left(\frac{\mathrm{SAT}}{\mathrm{SAT} + \gamma \cdot (Z_L - Z)}\right)^{\frac{g}{R\gamma}} \tag{3}$$

$$\mathrm{SAT}' = \mathrm{SAT} - \gamma \cdot (Z_L - Z) \tag{4}$$

where $g = 9.81\ \mathrm{m\ s^{-2}}$, $R = 287\ \mathrm{J\ K^{-1}\ kg^{-1}}$, and $\gamma = 0.007\ \mathrm{K\ m^{-1}}$. The corrected surface specific humidity (SSH', in kg kg^{-1}) is determined by the following formula (Bolton, 1980; Murray, 1967):

$$\mathrm{SSH}' = \mathrm{RH} \times 0.622 \times \frac{es}{\mathrm{SP}'} = \frac{\mathrm{RH} \times 0.622}{\mathrm{SP}'} \times \begin{cases} 6.1078 \exp\left[\dfrac{17.27\left(\mathrm{SAT}' - 273.16\right)}{\mathrm{SAT}' - 35.86}\right], & \mathrm{SAT}' \geq 273.16 \\ 6.112 \exp\left[\dfrac{17.67\left(\mathrm{SAT}' - 273.16\right)}{\mathrm{SAT}' - 29.66}\right], & \mathrm{SAT}' < 273.16 \end{cases} \tag{5}$$

where es is the saturation vapor pressure (hPa), and 0.622 (kg kg^{-1}) is the ratio of the molar mass of water vapor to dry air. The above correction could effectively fix the mean bias of atmospheric forcing data (particularly for WS) over large lakes like Lake Nam Co (Figure S1 in Supporting Information S1).

2.2.3. Satellite Data of LSWT

Here Moderate Resolution Imaging Spectroradiometer (MODIS/Terra) Land Surface Temperature (LST) product (MOD11A1; Wan et al., 2015) with a spatial resolution of 1 km during 2001–2018 is utilized to evaluate the LSWT simulations because it has a longer time span, more clear-sky pixels, and better performance over lake surface at night than MODIS/Aqua (Fu et al., 2011; Li et al., 2014; Quan et al., 2014). An evaluation study based on five TP large lakes (Lazhu et al., 2022) indicates that the MODIS LST agrees with in situ with an RMSE < 1 (2) °C during daytime (nighttime), where MODIS/Terra performs better than MODIS/Aqua during the lake's thermal stratification period.

First, we exclude the MODIS pixels with a distance of less than 1 km from the lake shoreline to avoid land contamination (Guo et al., 2022), and obtain the daily MODIS LSWT by averaging the two instantaneous observations at 10:30 and 22:30 local time. Note that we focus on LSWT variations during the ice-free summer months of July, August, and September, so daily LSWT values below 0°C are discarded for model evaluation. Then the spatial averaging is performed to derive the LSWT time series for each lake, and we remove the obvious outliers that exceed ±3 times the standard deviations of the respective annual time series for each day. This deriving series will be used to evaluate the simulations on the corresponding dates. Due to numerous missing values in the derived daily MODIS LSWT time series after quality control procedures, we applied linear interpolation over time to obtain a reliable LSWT interannual trend (Davis, 1975; Zhang et al., 2014). For example, in the case of Lake Nam Co, the estimated interannual trend from interpolated LSWT closely matches with that derived from the 8-day averaged MOD11A2 LSWT product (0.15 ± 0.44°C decade^{-1} vs. 0.14 ± 0.59°C decade^{-1}), indicating that the interpolation effectively preserves the trend characteristics.

2.3. WRF-Lake Model Description

WRF-Lake model is a 1-D mass and energy balance lake model derived from the eddy diffusion model developed by Henderson-Sellers (1985) and Hostetler and Bartlein (1990), with Subin et al. (2012) and Gu et al. (2015) further improving the representation of surface snow, ice, and bottom soil sediment processes. For better applicability to deep (>50 m) and brackish lakes over TP, Huang et al. (2019) and Wu et al. (2020) made a series

of modifications, for example, decreasing the temperature of maximal water density, adding dynamic parameterizations for surface roughness lengths, reducing the light extinction coefficient, and enlarging eddy diffusivity. Compared to FLake, which is another widely used two-layer model based on self-similarity theory and is designed for lower computational demand in simulating surface temperature and ice dynamics (Bernus et al., 2021; Huang et al., 2019; Mironov et al., 2010), we have chosen the WRF-Lake model for its specific advantages in simulating the vertical temperature structure in large deep lakes, because FLake relies on a simplified structure that often applies a "virtual bottom cutoff" at a shallow depth, typically around 50 m, limits its application in deep lake simulations.

Since most studied lakes are saline and salinity (S, in g L^{-1}) plays an important role in determining the water's thermal properties, for example, thermal conductivity, heat capacity, and freezing point, we implement a salinity parameterization scheme (Wen et al., 2015; Yusufova et al., 1975) into the WRF-Lake model, as formulated by:

$$\lambda_{sw} = \lambda_{fw}\left(1.0 - 2.3 \times 10^{-2}\mathrm{S} + 10^{-3}S^2\right) \tag{6}$$

$$Cp_{sw} = Cp_{fw} - 4.4S \tag{7}$$

$$T_f = 273.15 - 0.056\mathrm{S} \tag{8}$$

where λ_{sw} ($\lambda_{fw} = 0.6$) is the thermal conductivity for salt (fresh) water (in W m^{-1} K^{-1}), Cp_{sw} ($Cp_{fw} = 4.188 \times 10^3$) is the specific heat at constant pressure for salt (fresh) water (in J kg^{-1} K^{-1}), T_f is the freezing point for salt water (in K).

Besides the atmospheric forcing, lake-specific parameters like η and maximum ice albedo (α_{imax}) require further tuning to achieve reliable simulations (Huang et al., 2021; Wu et al., 2024). Therefore, we conducted a series of parameter-tuning simulations running from 1 June 2000 to 31 December 2018 to tune η and α_{imax} independently for each lake. Specifically, in these parameter-tuning simulations, α_{imax} is tuned over a range of 0.2–0.6 with a step of 0.01 for all lakes; η is multiplied by a scale factor (tuned over ranges 0.25–3.0 with a step of 0.05) on the initial η_0 calculated by Equation 1 for each lake (Huang et al., 2021). Finally, the value of η and α_{imax} that minimize daily mean absolute bias (AB, Wu et al., 2024) of LSWT will be determined as the optimal value (as listed in Table S1 of Supporting Information S1) to be used in the final control simulation and the following sensitivity simulations in the next section. Both AB and temporal correlation coefficient (TC, ranges −1–1) are used to evaluate the model performance:

$$\mathrm{AB} = \frac{1}{N}\sum_{i=1}^{N}|S_i - O_i| \tag{9}$$

$$\mathrm{TC} = \frac{\sum_{i=1}^{N}\left(S_i - \overline{S}\right)\left(O_i - \overline{O}\right)}{\sqrt{\sum_{i=1}^{N}\left(S_i - \overline{S}\right)^2}\sqrt{\sum_{i=1}^{N}\left(O_i - \overline{O}\right)^2}} \tag{10}$$

where $S_i(O_i)$ is the simulation (observation) at the ith time or space sample and $\overline{S}(\overline{O})$ is the average of simulation (observation) with a sample size of N. The smaller (larger) the absolute value of AB (TC), the better the simulation results (Wu et al., 2024).

The simulations for 81 selected lakes are done one-by-one and initialized with a uniform lake column water temperature of 4°C. The atmospheric forcings are updated every 10 min by linearly interpolating the corrected JRA-55 data. We take the model results in 1979 as a spin-up phase and use the results from 1980 onward for analysis.

2.4. Methods for Attributing LSWT Trend to Atmospheric Variables

2.4.1. Sensitivity of LSWT to Atmospheric Variables

We conduct a series of experiments using the change factor approach (Butcher et al., 2015; Magee & Wu, 2017) to examine the impacts of the climatic perturbations of each atmospheric variable on LSWT over the climatic mean state. For a forcing variable, while keeping other variables unchanged, we first compute the standard deviation of

the respective annual time series for each month (σ_m, $m = 1, 2, \ldots, 12$). Then, we add respective perturbation $\lambda_n\sigma_m$ to the base value for each month across all years. Here λ_n ranges from -2.0 to 2.0 with an increment of 0.2 and thus there are 21 sample experiments ($n = 1, 2, \ldots, 21$). The perturbation ranges are chosen according to the variables' change characteristics, ensuring they cover the actual extreme climate ranges and avoid unrealistic scenarios (Stetler et al., 2021).

From the above experiments, the $\overline{\mathrm{LSWT}}(\overline{F})$ series with a length of 21 can be derived by computing the climatic mean state for each of the 21 sample experiments corresponding to a given forcing variable F, where the overbar indicates the climatic mean. We then define the climatic response of LSWT to F, denoted by $\frac{\partial\overline{\mathrm{LSWT}}}{\partial\overline{F}}$, as the absolute sensitivity S_a (S_a–F hereafter for brevity). Additionally, because the nth experiments with the same λ_n have the same relative magnitude of climate perturbation for all variables, the relative sensitivity $S_r = \sigma S_a$ (σ is the standard deviation of the annual mean time series for F) can be defined to compare the relative magnitude that LSWT responds to each forcing variable under a perturbation of 1σ. An example of the sensitivity analysis is Lake Nam Co on TP (Shi et al., 2022).

2.4.2. Contributions of the Atmospheric Forcing Variables to the LSWT Trend

We use the partial derivative decomposition method to estimate the contributions of atmospheric forcing variables to the LSWT trend (Roderick et al., 2007; Shi et al., 2022; Yan et al., 2019). Assuming that to first order, the LSWT trend $\left(\frac{d\mathrm{LSWT}}{dt}\right)_F$ responds linearly to the changes of atmospheric forcing variables (Austin & Colman, 2007), as decomposed by:

$$\left(\frac{d\mathrm{LSWT}}{dt}\right)_F \approx \sum_i \frac{\partial \mathrm{LSWT}}{\partial F_i}\frac{dF_i}{dt} \approx \sum_i S_{ai}\frac{dF_i}{dt} \tag{11}$$

where F_i and $\frac{dF_i}{dt}$ are the ith atmospheric forcing variable and its long-term trend, respectively. $\frac{\partial\mathrm{LSWT}}{\partial F_i}$ is the LSWT change resulting from F_i and could be approximated as the absolute sensitivity S_{ai} (Shi et al., 2022). Consequently, $S_{ai}\frac{dF_i}{dt}$ is defined as the synthesis contribution (SC) of F_i to the LSWT trend. $\sum_i S_{ai}\frac{dF_i}{dt}$ is defined as the estimated LSWT trend, which is used as the denominator for calculating the contribution rate from each forcing variable, that is, the contribution rate of F_i is $S_{ai}\frac{dF_i}{dt}/\sum_i S_{ai}\frac{dF_i}{dt} \times 100\%$.

Note that the decomposition method operates on the principle that the atmospheric variables are independent of each other. However, although they are treated as independent inputs in the model, atmospheric variables are indeed coupled and interact mutually in the climate system. Hence, $\frac{dF_i}{dt}$ is affected by the interactions represented by the interannual collinearity among atmospheric variables. The synthesis contribution (SC) of F_i to the LSWT trend consists of the individual contribution (IC) and the cross contribution (CC) from interactions among atmospheric variables, that is, SC = IC + CC.

To detach the IC from the SC, we first use zero-phase component analysis (ZCA) to decorrelate the original atmospheric variables $\boldsymbol{F}$ to obtain mutually independent (no linear correlation) atmospheric variables $\boldsymbol{Z}$ (Shi et al., 2022). Specifically, the original matrix $\boldsymbol{F}_{p\times s}$ with p variables and s years is standardized to $\boldsymbol{F}^*$. Each row $F_i^* = \frac{F_i - \overline{F}_i}{\sigma_i}$ represents the ith standardized atmospheric forcing variable, where $\overline{F}_i$ and σ_i are the mean value and standard deviation, respectively. Then, we perform a linear transform $\boldsymbol{W}$ on $\boldsymbol{F}^*$ to obtain the standardized $\boldsymbol{Z}$, denoted as $\boldsymbol{Z}^*$:

$$\boldsymbol{Z}^* = \boldsymbol{W}\boldsymbol{F}^* = \left(\boldsymbol{U}\boldsymbol{\Lambda}^{-\frac{1}{2}}\boldsymbol{U}^T\right)\boldsymbol{F}^* \tag{12}$$

where $\boldsymbol{W} = \boldsymbol{U}\boldsymbol{\Lambda}^{-\frac{1}{2}}\boldsymbol{U}^T$ is termed ZCA transformation or Mahalanobis transformation, $\boldsymbol{U}$ and $\boldsymbol{\Lambda}$ are the orthogonal and diagonal matrix resulting from the eigenvalue decomposition of the covariance matrix of $\boldsymbol{F}^*$. For more details about ZCA transformation, refer to Bell and Sejnowski (1997) and Kessy et al. (2018). Finally, $\boldsymbol{Z}^*$ is transformed back to the original physical magnitude to obtain the independent (decorrelated) variables $\boldsymbol{Z}$ with each row

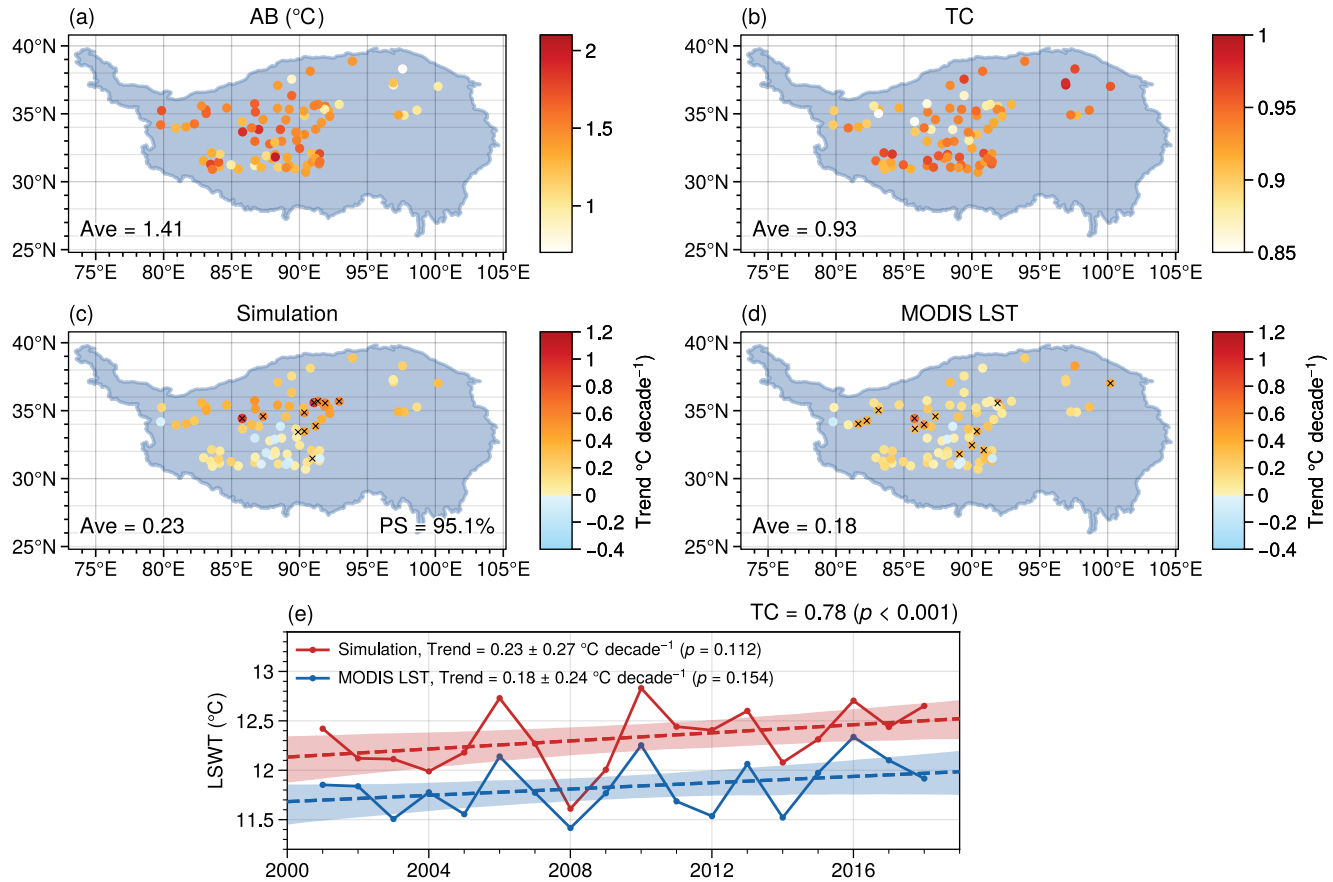

Figure 2. Spatial distributions of the (a) average absolute bias (AB) and (b) temporal correlation coefficient (TC) of simulated summer daily LSWT (for all times with LSWT >0°C) relative to MODIS. Spatial distribution of the short-term trends of summer LSWT for (c) simulation and (d) MODIS during 2001–2018, with PS denoting the proportion of lakes sharing the same trend direction, Ave denoting the averaged value across all studied lakes and the black cross indicating the significance at $p < 0.05$ level. (e) Interannual variation and short-term trend of 81 lakes-averaged LSWT for simulation (red) and MODIS (blue), and shaded areas indicate the 95% confidence interval for the regression estimate.

$Z_i = Z_i^* \sigma_i + \overline{F}_i$. Here, the correlation coefficients among the rows of $\boldsymbol{Z}$ are small, but the interannual variations of rows are close to the original data $\boldsymbol{F}$.

By substituting $\boldsymbol{Z}$ for $\boldsymbol{F}$ in Equation 11, we obtain

$$\left(\frac{d\text{LSWT}}{dt}\right)_Z \approx \sum_i \frac{\partial \text{LSWT}}{\partial Z_i}\frac{dZ_i}{dt} \approx \sum_i S_{ai}\frac{dZ_i}{dt} \tag{13}$$

where $S_{ai}\frac{dZ_i}{dt}$ could be understood as the IC of F_i, because $\frac{dZ_i}{dt}$ does not contain the interactions among atmospheric forcing variables. Accordingly, CC from the interaction of F_i and other variables is calculated as the difference between its SC and IC, that is, $S_{ai}\frac{dF_i}{dt} - S_{ai}\frac{dZ_i}{dt}$, and the total CC from interactions among all atmospheric forcing variables is calculated as $\sum_i \left(S_{ai}\frac{dF_i}{dt} - S_{ai}\frac{dZ_i}{dt}\right)$.

It should be clarified that CC = SC–IC is derived from $\frac{dF_i}{dt} - \frac{dZ_i}{dt}$ and represents the contribution of F_i due to the interaction of F_i with other variables. However, the effect of this interaction on LSWT is ultimately reflected by F_i through the lake surface energy balance. In other words, CC and IC are discussed from the perspective of the atmosphere system, while SC is the direct expression from the perspective of the lake system.

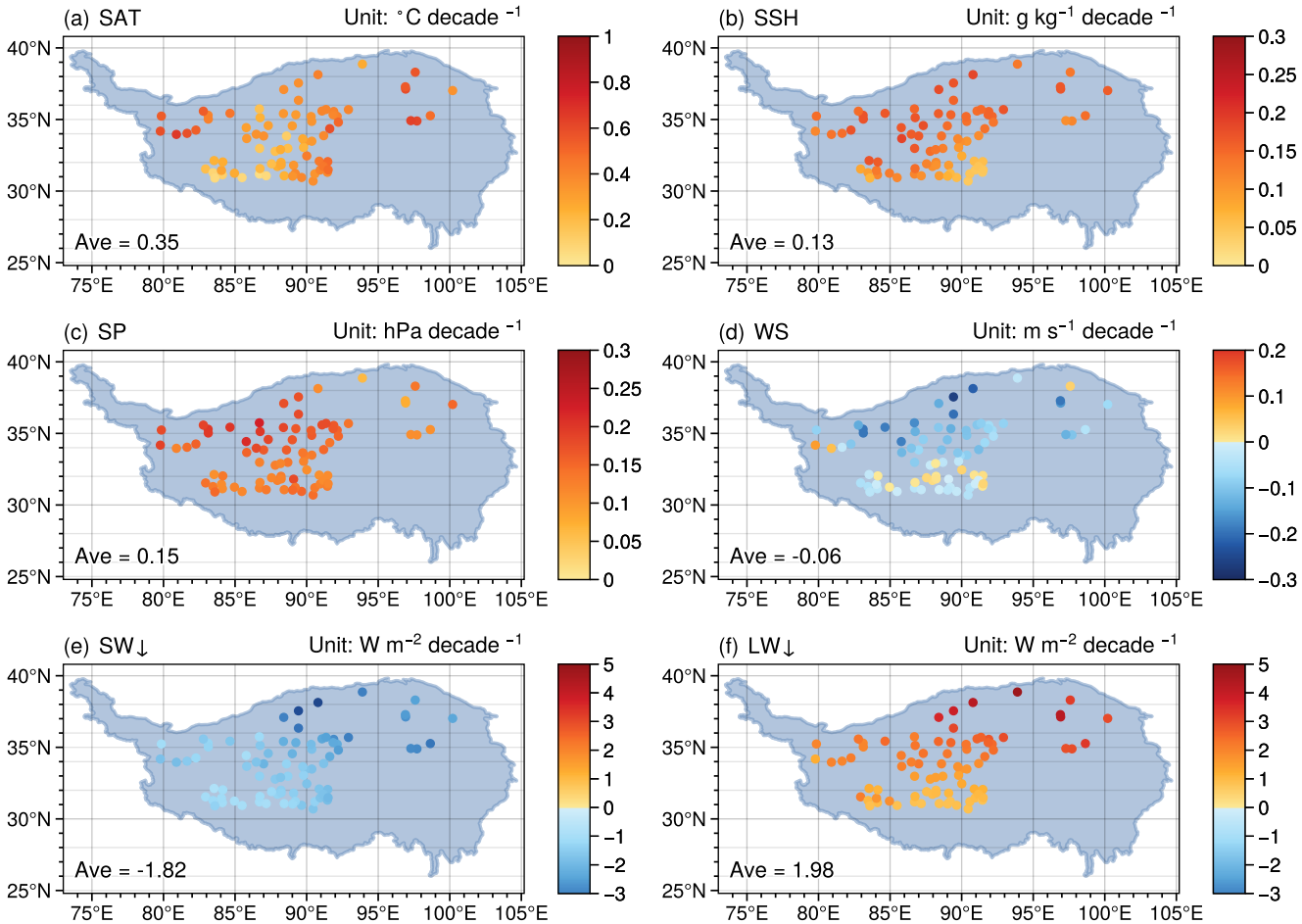

Figure 3. Spatial distribution of long-term trend of annual atmospheric forcing after corrected: (a) surface air temperature (SAT), (b) surface specific humidity (SSH), (c) surface pressure (SP), (d) 10 m wind speed (WS), (e) downward shortwave radiation ($SW_{\downarrow}$), and (f) downward longwave radiation ($LW_{\downarrow}$). Ave denotes the averaged value across all studied lakes.

3. Results

3.1. Model Validation

Figure 2 shows the spatial map of evaluation metrics (AB and TC) for daily LSWT from simulations relative to the MODIS observations across all studied lakes during 2001–2018, as well as the short-term interannual trends. From Figures 2a and 2b, WRF-Lake shows good performance in simulating the magnitude and temporal evolution of LSWT during summer months (July, August, and September), yielding an average AB of 1.44°C and TC of 0.93. The high TC is both contributed by the seasonal cycle and interannual variability of LSWT (Figure 2e). Next, we compare the simulated and observed short-term interannual trends of summer LSWT (Figures 2d and 2e). According to MODIS, 75 (92.6%) of the studied lakes show an increasing LSWT trend during 2000–2018, with an average interannual trend of 0.18°C decade^{-1} averaged over all studied lakes. The model well replicates the overall increase of LSWT with an interannual trend of 0.23°C decade^{-1}. Between the simulations and observations, 77 (95.1%) of the studied lakes share the same trend direction, and there is also good consistency in the lakes-averaged interannual variations (TC = 0.78). The trend bias in the remaining 4 lakes (4.9%) is mainly from the uncertainty due to the short time series used for calculations and trend values close to 0. Consequently, the simulation captures the spatial and temporal characteristics of short-term LSWT trends well.

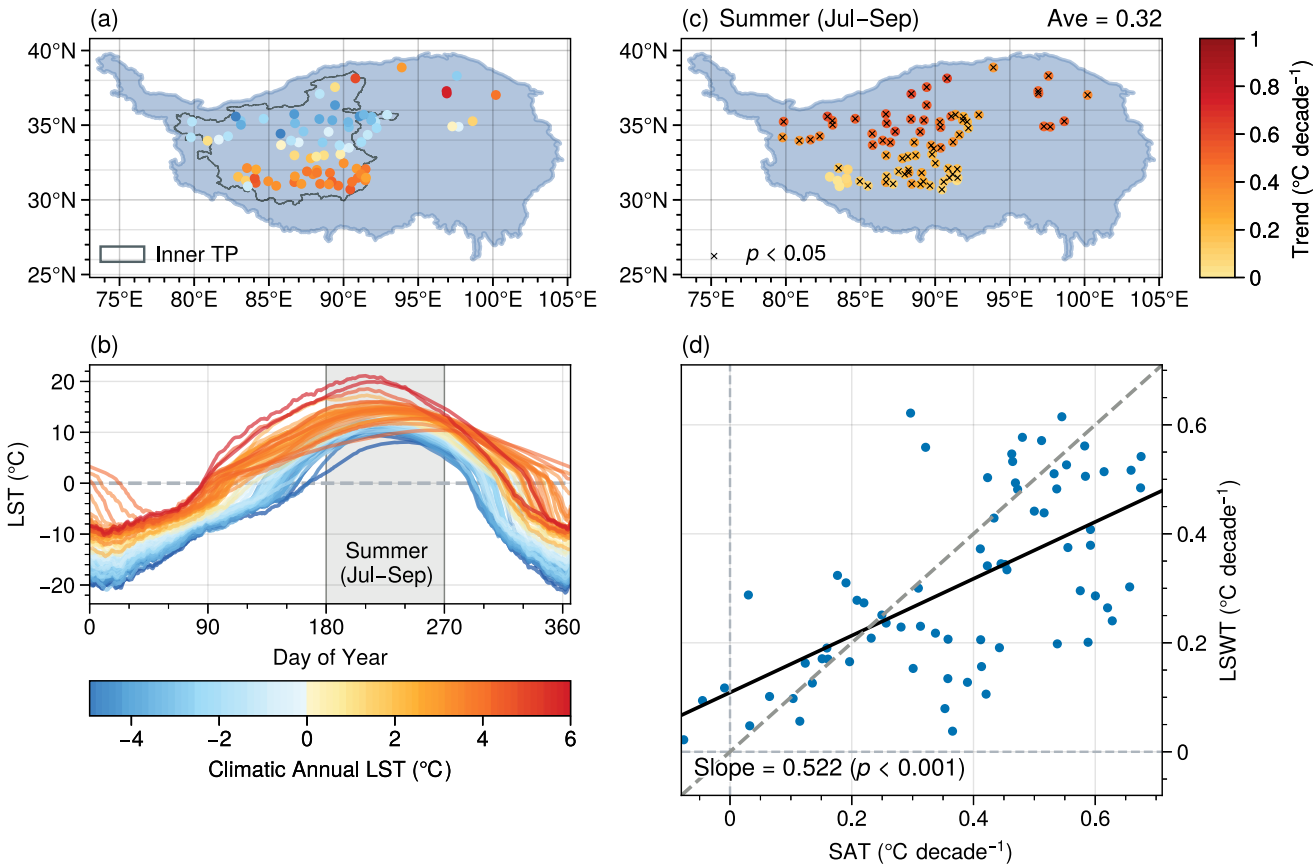

Figure 4. (a) Climatic annual averages, (b) daily climatic variations, and (c) long-term summer trends of simulated lake surface temperature (LST) during 1980–2018; (d) regression relationships between the long-term summer trends of LSWT and SAT. The gray zone in (b) denotes the summer months of July, August, and September. The black cross in (c) indicates the significance at $p < 0.05$ level.

3.2. Long-Term Trends of Atmospheric Forcing Variables and LSWT

Figure 3 shows the distribution of long-term trends of corrected atmospheric forcings. A consistent pattern of increasing SAT, SSH, SP, $LW_{\downarrow}$, and decreasing $SW_{\downarrow}$ can be found across all studied lakes, with lake-averaged long-term trends of 0.35°C decade^{-1}, 0.13 g kg^{-1} decade^{-1}, 0.15 hPa decade^{-1}, 1.98 W m^{-2} decade^{-1}, and −1.82 W m^{-2} decade^{-1}, respectively. WS shows a weakening trend over most TP lakes, except for 16 (19.8%) lakes in southern TP, and the long-term trend averaged over all studied lakes is −0.06 m s^{-1} decade^{-1}. These climate changes are in agreement with previous studies (Kuang & Jiao, 2016; Yang et al., 2014) and expected to have a significant impact on long-term changes in LSWT.

Figures 4a and 4b show the climatic averages and climatic annual cycle of simulated lake surface temperature (LST) for the studied 81 lakes during 1980–2018, with the long-term trends of summer LSWT and SAT shown in Figures 4c and 4d. Note that LST is calculated as the average of ice surface temperature and LSWT weighted by ice concentration, and exactly equals LSWT during the summer ice-free months. A remarkable difference in the LST regime can be found between lakes situated north and south of ~33°N over inner TP: (a) the climatic mean LST is below 0°C over the northern TP but above 0°C over southern TP (Figure 4a); (b) lakes over northern TP feature a more prolonged ice-covered phase and evidently lower summer LSWT (Figure 4b); and (c) the average increasing rate of summer LSWT is much higher over northern TP than over southern TP (0.44 vs. 0.16°C decade^{-1}, Figure 4c). The overall warming trends range from 0.01 to 0.62°C decade^{-1}, with an average value of 0.32°C decade^{-1}, which is slightly smaller than the global mean increasing rate of summer LSWT during 1985–2009 (0.34°C decade^{-1}, O'Reilly et al., 2015). From Figure 4d, only 26 (32.1%) lakes in our study have a higher warming rate than the ambient air in summer, and the average lake warming rate (0.32°C decade^{-1}) is only 78.5% of the air warming rate (0.41°C decade^{-1}). This is different from the global analysis that most seasonally ice-

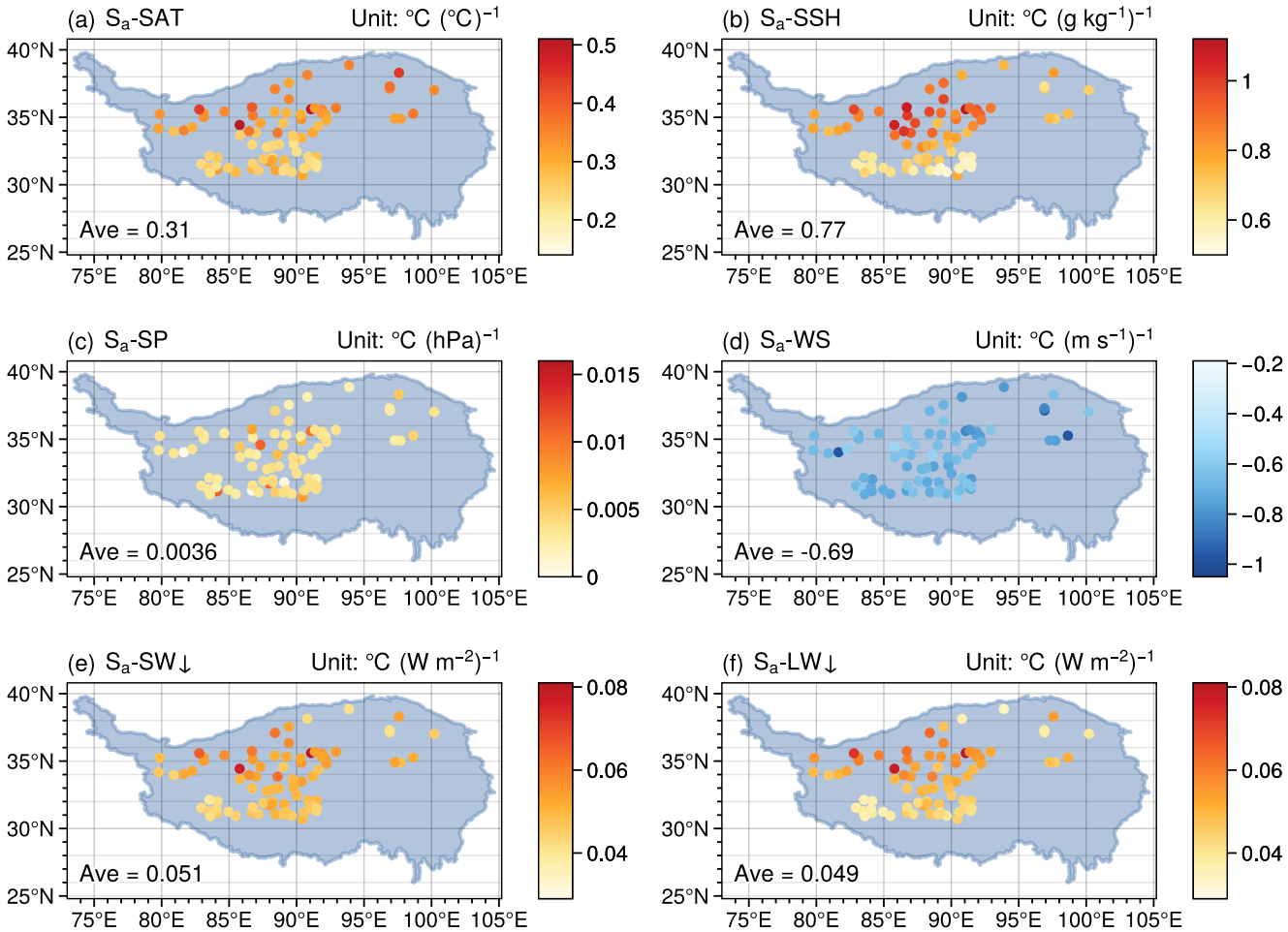

Figure 5. Spatial distribution of absolute sensitivity S_a of LSWT to (a) surface air temperature (S_a–SAT), (b) surface specific humidity (S_a–SSH), (c) surface pressure (S_a–SP), (d) 10 m wind speed (S_a–WS), (e) downward shortwave radiation (S_a–SW$_\downarrow$), and (f) downward longwave radiation (S_a–LW$_\downarrow$). Ave denotes the averaged value of S_a–F across all studied lakes.

covered lakes warmed faster than the local air due to the positive ice-albedo feedback (Huang et al., 2023; O'Reilly et al., 2015).

3.3. Sensitivity of Summer LSWT to Perturbation of Atmospheric Forcing Variables

Next, we will quantify the impacts of atmospheric variables on LSWT and their contribution to LSWT trends via sensitivity analyses. Figure 5 shows the absolute sensitivity S_a of LSWT, which indicates the LSWT change corresponding to a unit perturbation of atmospheric variables on their climatic mean state. Figure 6 shows the relative sensitivity S_r–F, which indicates the change in climatic mean LSWT after per unit standard deviation of perturbation in atmospheric forcing variables.

As seen in Figure 5, LSWT increases with the increasing thermodynamic variables (i.e., SAT, SSH, LW$_\downarrow$, and SW$_\downarrow$), decreases with the increasing wind speed, and shows little response to the slight perturbation of SP for all studied lakes. Among the 81 lakes studied, the sensitivities of LSWT to SAT, denoted as S_a–SAT, are less than 1°C °C^{-1}. On average, S_a–SAT = 0.31°C °C^{-1}, meaning that each increment of 1°C in SAT causes an increment of just 0.31°C in LSWT. The average values of S_a–SSH and S_a–WS are 0.77°C (kg kg^{-1})$^{-1}$ and −0.69°C (m s^{-1})$^{-1}$, respectively. S_a–SW$_\downarrow$ and S_a–LW$_\downarrow$ are comparable with the average values of 0.051 and 0.049°C (W m^{-2})$^{-1}$, respectively. The sensitivities to thermodynamic variables, for example, S_a–SSH and S_a–LW$_\downarrow$, show noticeable north–south disparities, implying that LSWT over northern TP is more sensitive to perturbations of thermodynamic variables than that over southern TP. Regarding the response of climatic mean LSWT to different

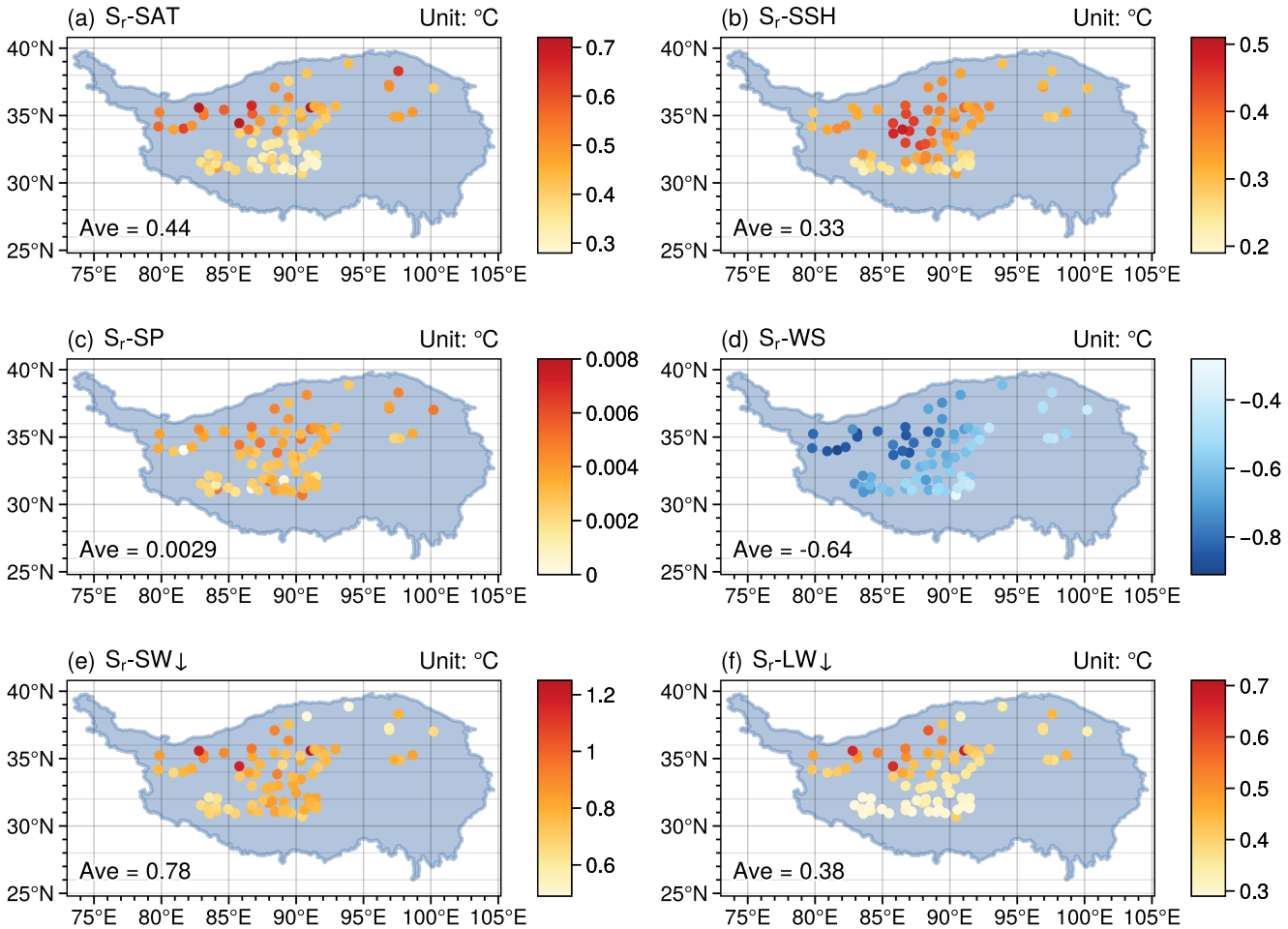

Figure 6. Same as Figure 5, but for the relative sensitivity S_r.

atmospheric forcing variables (Figure 6), $SW_{\downarrow}$ and WS exert the most significant impacts with mean S_r values of 0.78°C and −0.64°C averaged over all studied lakes, followed by SAT (0.44°C), $LW_{\downarrow}$ (0.38°C), and SSH (0.33°C). The influence of SP is negligible. S_r–F exhibits more pronounced north–south disparities than S_a–F except for SP.

The primary reason for the north–south disparities in S_a and S_r for thermodynamic variables lies in the climatic difference across TP. First, both air temperature and radiation intensity are weaker over northern TP, leading to a colder climate and lower climatic mean LSWT (Figure 4). Moreover, S_a for atmospheric thermodynamic variables (S_a–F) is significantly correlated with the climatic mean forcing variables ($\overline{F}$), and the correlation coefficients between S_a–F and $\overline{F}$ are −0.42, −0.60, −0.40, and −0.77 for SAT, SSH, $SW_{\downarrow}$, and $LW_{\downarrow}$, respectively. Larger S_a is associated with lower climatic SAT SSH, $SW_{\downarrow}$, and $LW_{\downarrow}$, or in other words, S_a are larger in the colder lakes under colder climates, for example, northern inner TP lakes in Figure 4a. According to Equation 11, when the SAT trend and other atmospheric variables remain unchanged, a larger S_a–SAT resulting from lower SAT causes a greater contribution of SAT to the LSWT trend. This is similar to other atmospheric thermodynamic variables and aligns with previous studies that suggest the warming trends of lakes under colder climates are amplified under the same forcing trend (O'Reilly et al., 2015; Shi et al., 2022). These results reveal that the LSWT trends of TP lakes depend not only on the trends of atmospheric variables but also on their climatic state.

3.4. Contributions of Atmospheric Variables to the Long-Term Summer LSWT Trend

Before qualifying the contribution of atmospheric variables, we first estimate the long-term summer LSWT trends using Equation 11 and compare them with the simulated summer LSWT trends (Figure 7). The estimated and

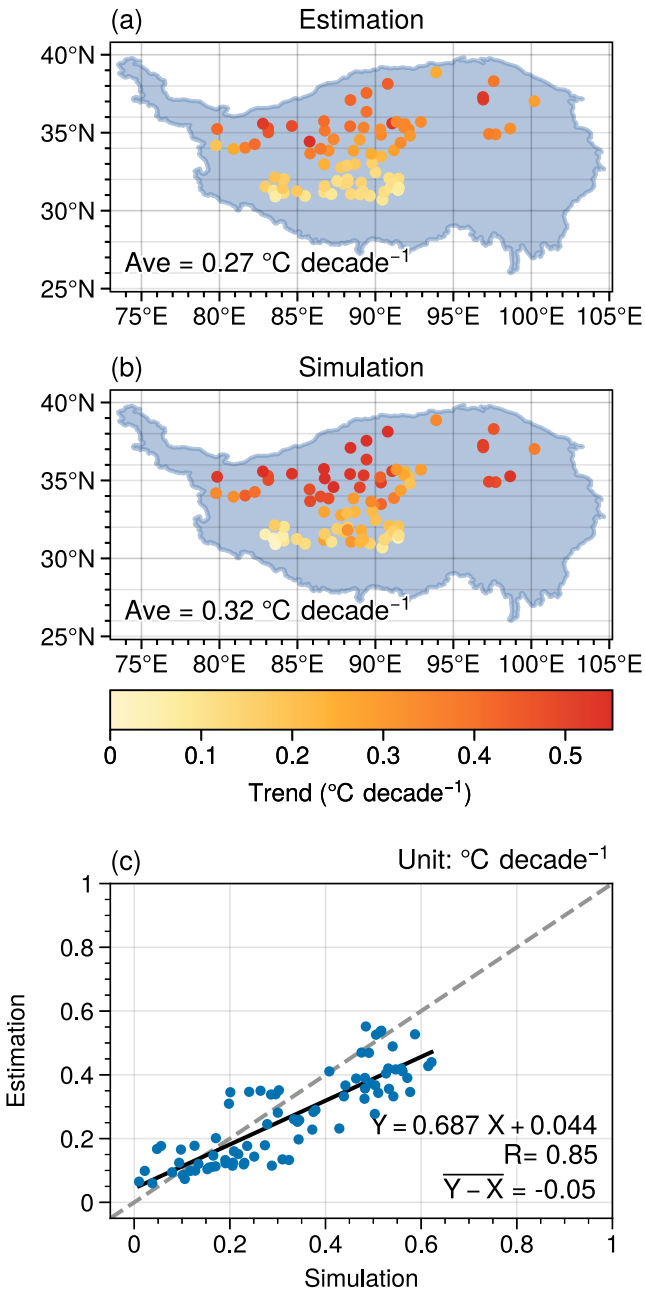

Figure 7. Spatial distributions of (a) estimated and (b) simulated long-term summer LSWT trends during 1980–2018, with the averaged value (Ave) across all the studied lakes; (c) their regression relationship, with the linear regression equation, R, and mean bias of estimation relative to simulation ($\overline{Y - X}$).

simulated LSWT trends show similar spatial distributions, increasing from south to north, with an R value of 0.85 (Figures 7a and 7b). However, the mean estimated trend of 0.27°C decade^{-1} is lower than the mean simulated trend of 0.32°C decade^{-1}. The underestimation is more pronounced for the lakes located in higher altitude and latitude regions, which are found to undergo more pronounced warming. Despite the underestimation, the estimation and simulation display a good linear relationship (Figure 7c). While we could have corrected the estimation using the regression equation, it does not change the calculation of the contribution percentages, so it can be omitted.

Figure 8 illustrates the synthesis contribution (SC) of each atmospheric forcing variable to long-term summer LSWT trends. From the perspective of lake system, SC should be interpreted as the ultimate contribution of each atmospheric variable to the long-term summer LSWT trends through the lake surface energy balance. SC of atmospheric variables shows distinct spatial variations. The SC of SAT is positive and notably larger in the northern TP lakes compared to the central and southwestern TP lakes; the positive SC of SSH decreases from northwest to southeast; SC of WS is positive over the northern TP, but it is reduced or occasionally even negative over the southern TP; The SC of $SW_{\downarrow}$ ($LW_{\downarrow}$) is generally negative (positive) for all the studied lakes and shows larger absolute values in the northern TP. SC of SP is ignored due to its slight influence. For the average of the 81 lakes, the SC of SAT, SSH, and $LW_{\downarrow}$ is comparable with the values around 0.1°C decade^{-1}, contributing positively by 41.6%, 39.0%, and 37.7% to the total summer LSWT trend, respectively, followed by the SC of WS (0.045°C decade^{-1}, 16.8%). This suggests that the air warming (including increases in SAT and $LW_{\downarrow}$) and wetting over the TP are the primary drivers for lake warming. Moreover, it is worth noting that the negative contribution is solely due to the SC of SW↓ (−0.09°C decade^{-1} with a −35.1% contribution of the total summer LSWT trend), which almost offsets the warming contribution of LW↓ and therefore slows down lake warming.

From the perspective of atmosphere system, SC should be divided into individual contribution (IC) and cross contribution (CC), reflecting the influences from independent changes of each variable and interactions among all variables, respectively. Figure 9 shows the distribution of IC of each atmospheric variable and the total cross contribution (CC) of all variables. IC of SAT is positive and notably larger in the lakes over eastern and western TP than in the lakes over north-central and southwestern TP, where some even show negative IC; The positive IC of SSH decreases from west to east; IC of WS is negative (positive) in the lakes over the southwestern (northern and eastern) TP; IC of $SW_{\downarrow}$, $LW_{\downarrow}$, and total CC are generally negative, positive, and positive for all studied lakes, respectively, with larger absolute values in northern TP. For the average of 81 lakes, total CC is 0.149°C decade^{-1} and has a positive contribution of as much as 55.1% to the long-term summer LSWT trends, followed by IC of $LW_{\downarrow}$ (0.082°C decade^{-1}, 30.3%), SSH (0.039°C decade^{-1}, 14.3%), SAT (0.040°C decade^{-1}, 14.8%), and WS (0.018°C decade^{-1}, 6.6%). Mean IC of $SW_{\downarrow}$ is −0.057°C decade^{-1} and has a negative contribution of −21.1%. This suggests that the enhanced atmospheric forcing trends due to the interaction among atmospheric variables contribute to more than half of the lake warming.

From the perspective of lake system, the interaction among atmospheric variables still influences the lake system through each individual variable. Next, we examine the CC of individual variables to long-term summer LSWT trends (Figure 10). The interaction among atmospheric variables is mainly reflected by the CC of SAT and SSH (Figures 10a and 10b), with the mean values of 0.072 and 0.068°C decade^{-1}, contributing positively by 26.8% and 24.8% to the lake warming and accounting for a combined 93.6% of the total CC (0.149°C decade^{-1}, Figure 9f).

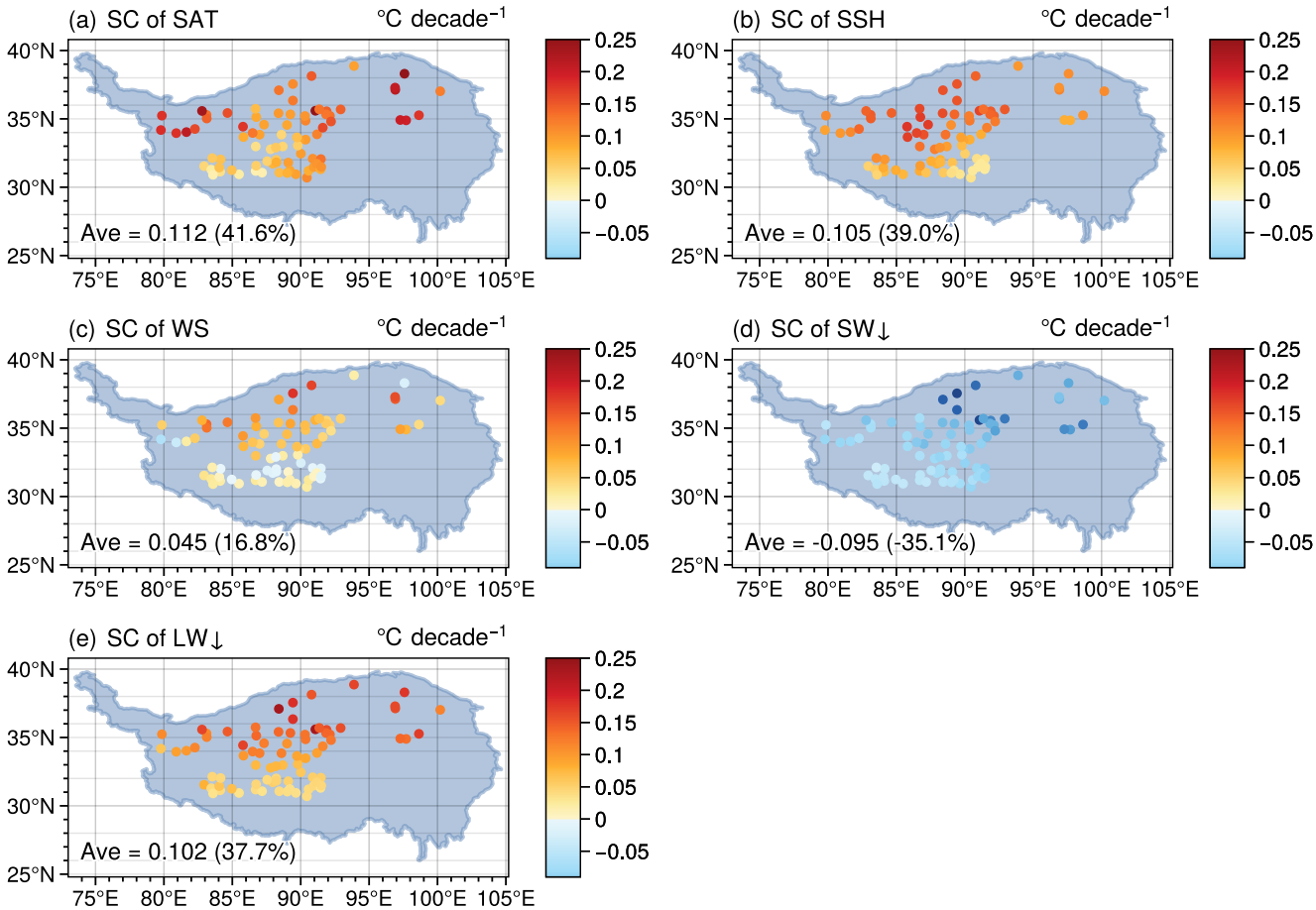

Figure 8. Spatial distributions of synthesis contribution (SC) of (a) surface air temperature (SAT), (b) surface specific humidity (SSH), (c) 10 m wind speed (WS), (d) downward shortwave radiation ($SW_{\downarrow}$), and (e) downward longwave radiation ($LW_{\downarrow}$). Ave denotes the averaged value across all the studied lakes, with the contribution rate to long-term summer LSWT trends given in parentheses.

Moreover, the CC of SAT and SSH show larger values in the northern TP than in the southern TP. The mean CC of WS, $SW_{\downarrow}$, and $LW_{\downarrow}$ is 0.028°C decade^{-1} (10.2%), −0.038°C decade^{-1} (−14.0%), and 0.020°C decade^{-1} (7.3%), respectively, with little spatial variability (Figures 10c–10e). In short, the contribution of interaction among atmospheric variables is also manifested in the air warming and wetting, which is consistent with the results from the SC analyses.

4. Discussion

4.1. Lakes Warming Faster in Northern TP Than Southern

In this study, we use the 1-D WRF-lake model to analyze the long-term summer LSWT trends for 81 large lakes over TP during 1980–2018. The simulated warming trends range from 0.01 to 0.62°C decade^{-1}, with an average of 0.32°C decade^{-1}, which is slightly smaller than the global average rate of lake warming (0.34°C decade^{-1}) during the summers of 1985–2009. The warming trends of TP lakes show a remarkable south–north difference, which, according to Equation 11, can be explained by the south–north difference in the long-term trend (Figure 3) and absolute sensitivity S_a (Figure 5) of atmospheric thermodynamic variables. It is necessary to note that the south–north difference in S_a is an intrinsic climatic feature and independent of the atmospheric data source, whereas the difference in forcing trend varies with different atmospheric forcing data. For example, Guo et al. (2022) and Huang et al. (2023) used other forcing data and obtained a different conclusion from this study, finding that lakes in the southern TP are warming faster. Absolute sensitivity $S_a = \frac{\partial \overline{\mathrm{LSWT}}}{\partial \overline{F}}$ mainly correlates with the climatic mean values of atmospheric thermodynamic variables instead of their long-term trends, and S_a is

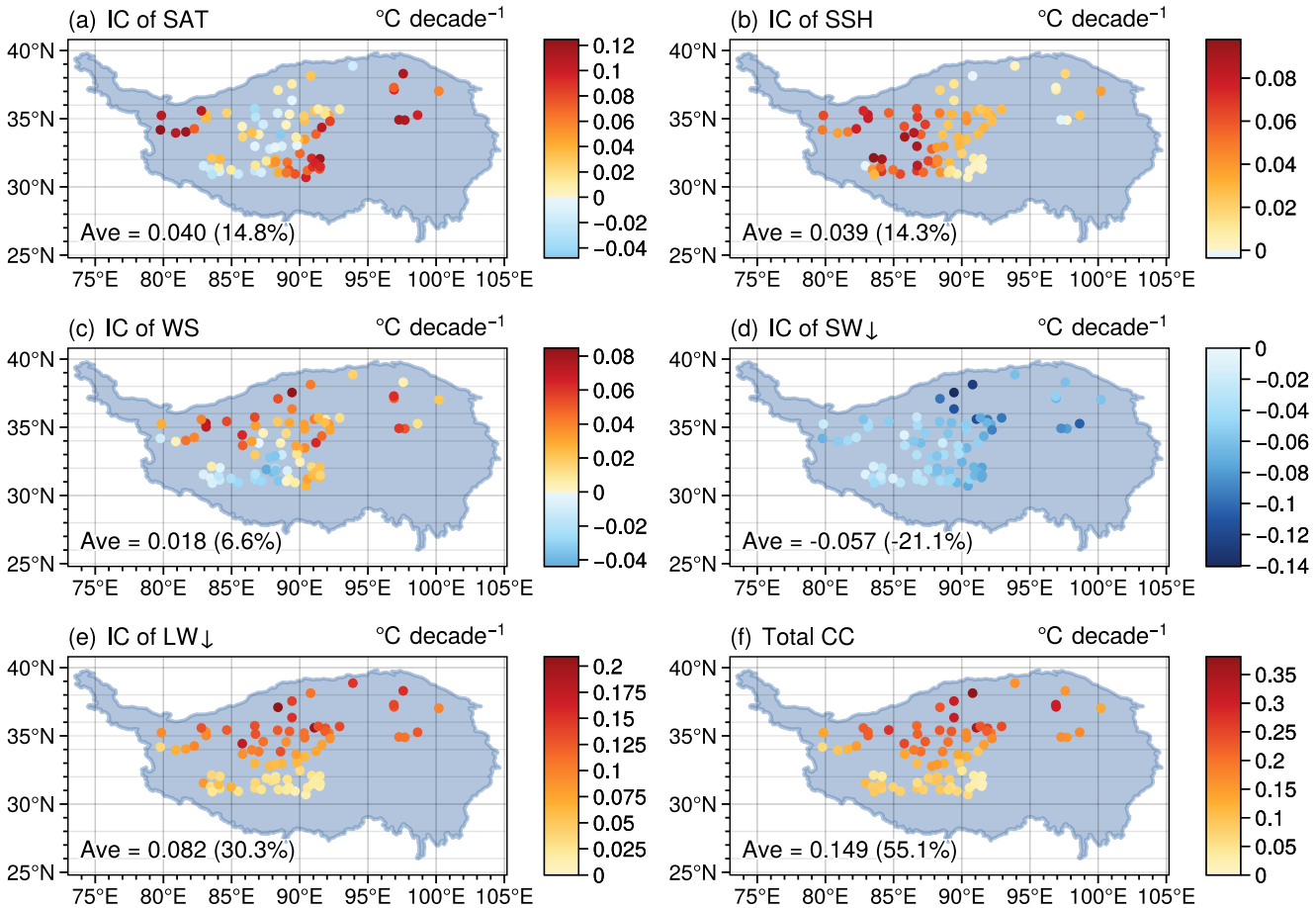

Figure 9. Spatial distributions of individual contribution (IC) of (a) surface air temperature (SAT), (b) surface specific humidity (SSH), (c) 10 m wind speed (WS), (d) downward shortwave radiation ($SW_{\downarrow}$), and (e) downward longwave radiation ($LW_{\downarrow}$), as well as (f) total cross contribution (CC) from interactions among all atmospheric forcing variables. Ave denotes the averaged value across all the studied lakes, with the contribution to long-term summer LSWT trends given in parentheses.

larger in colder lakes (in northern TP) with longer ice-covered phases (Figure 5). For instance, under the same increment of climatic SAT ($\overline{SAT}$), the increment of climatic LSWT ($\overline{LSWT}$) would be larger in colder lakes than in warmer lakes. This might be explained by the stronger surface evaporative cooling feedback in warmer lakes thus attenuating further warming (Tong et al., 2023; Zhou et al., 2023), which might impact the timing of ice-off and thermal stratification in seasonally ice-covered lakes. Understanding why warm lakes are less sensitive to atmosphere changes requires more comprehensive energy budget analyses.

4.2. Impacts of Atmospheric Variables on LSWT Trend

4.2.1. Warming and Wetting Over TP Dominates Lakes Warming

The contributions of atmospheric variables to summer LSWT trends are quantified from different perspectives. From the perspective of lake system, SC is considered as the contribution of atmospheric variables to LSWT trends through lake surface energy balance. For the TP lakes maintaining an unstable lake-air boundary layer (Wen et al., 2016), the rising SAT can decrease the upward sensible heat flux (SH) by reducing the lake-air temperature, and increase the upward latent heat flux (LH) by increasing the water surface saturation deficit; the increasing SSH can reduce the upward LH by saturating the surface air (Lang et al., 2021; Lazhu et al., 2016); the decreasing WS can not only reduce the upward SH and LH but also intensify the thermal stratification by weakening vertical mixing (Huang et al., 2012; Woolway et al., 2019); decreasing $SW_{\downarrow}$ and increasing $LW_{\downarrow}$ directly change the absorbed energy by lake. From the quantitative SC, air warming and wetting dominate the lake warming over TP, and SAT is the primary factor with a contribution rate of 41.6%, followed by SSH (39.0%) and

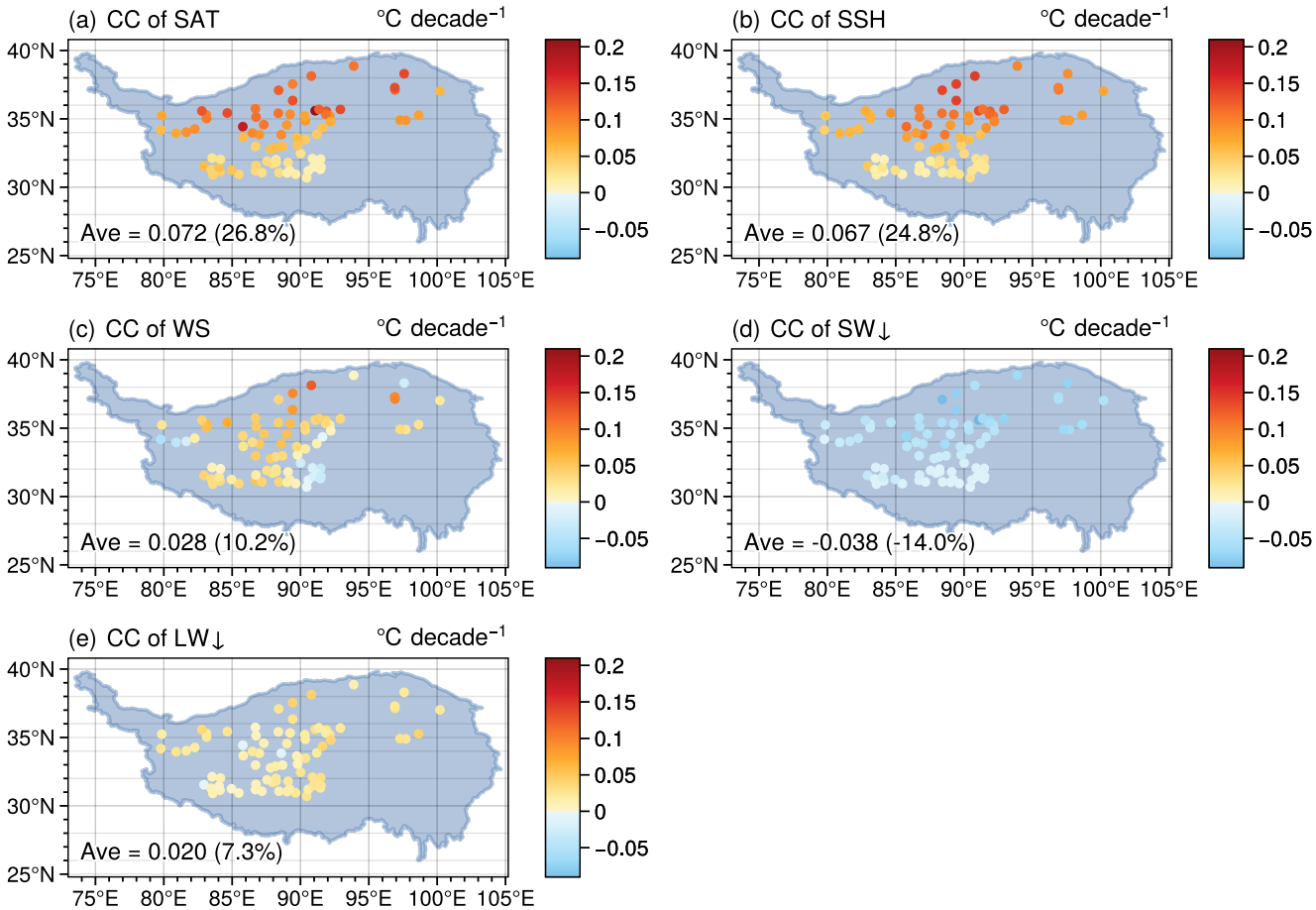

Figure 10. Same as Figure 8, but for the spatial distributions of cross contribution (CC) of SAT, SSH, WS, $SW_{\downarrow}$, and $LW_{\downarrow}$. The sum of the five terms is the total CC in Figure 9f.

$LW_{\downarrow}$ (37.7%). From the perspective of atmosphere system, the total CC from interactions among atmospheric variables exceeds half of the total contribution (55.1%), which highlights the complexity of changes in the climate system. It is worth noting that the CC of SAT and SSH account for 93.6% of the total CC, again indicating that the warming and wetting over TP is a crucial factor in lake warming, from both the perspective of lake and atmosphere systems.

It is important to emphasize that changes in the climate system are so complex, and atmospheric variables do not change completely independently. As in most studies (Li et al., 2019; Tong et al., 2023; Woolway et al., 2019), the effect of each variable F on LSWT is examined by conducting sensitivity experiments altering F while keeping the others unchanged. For example, SAT and $LW_{\downarrow}$ are treated as two independent atmospheric forcing variables in the lake model, and we separately calculate their sensitivities (S_a, S_r) and contributions to LSWT changes. However, from the perspective of atmosphere system, $LW_{\downarrow}$ is highly dependent on SAT according to the Stephens-Boltzmann relationship, that is, $LW_{\downarrow} \propto SAT^4$. Schmid et al. (2014) indicated that lake surface equilibrium temperatures were predicted to increase by 70%–85% of the increase in air temperature, which included the effect of $LW_{\downarrow}$ change. In our study, the LSWT only increases by 31% of the increase of SAT in climate state and the contribution rate of SAT to long-term summer LSWT trend is 41.6%. If the contribution of $LW_{\downarrow}$ is also considered as a part of SAT, the total contribution of SAT would be up to 79.3%.

Based on the quantitative CC, interactions among atmospheric variables are primarily reflected in the correlation between SAT and SSH (Figures 10a and 10b). According to the temporal correlation coefficients (TC) among atmospheric variables (Figure S2 in Supporting Information S1), the strongest correlation is the negative relationship between $SW_{\downarrow}$ and $LW_{\downarrow}$ (TC = −0.83), highlighting their nearly opposite contributions to the LSWT

trend. Additionally, SSH shows a positive correlation with $LW_{\downarrow}$ (TC = 0.82) and a negative correlation with $SW_{\downarrow}$ (TC = −0.78), as seen in the CC of SSH. Physically, increased water vapor results in more cloud cover, which reduces $SW_{\downarrow}$ (Yang et al., 2012) while enhancing $LW_{\downarrow}$ at the surface through the greenhouse effect (Ruckstuhl et al., 2007). There is also a positive correlation between SAT and $LW_{\downarrow}$ (TC = 0.74), which is explained by the Stefan-Boltzmann relationship, and this interaction is reflected in the CC of SAT.

4.2.2. Weakening Shortwave Radiation Slows Down Lakes Warming

It is interesting to note that only the weakening $SW_{\downarrow}$ leads to a negative contribution to the long-term increasing trends of summer LSWT, thereby slowing down the lakes warming over TP. In our results, only 26 (32.1%) of the studied lakes show a higher warming rate than the ambient air, which contrasts with findings that LSWT of seasonally ice-covered lakes generally increases more rapidly than the ambient air temperature (O'Reilly et al., 2015). In fact, the $SW_{\downarrow}$ increase has been observed globally in many lake-rich regions, for example, Europe (Schmid & Köster, 2016), East Asia (Shinohara et al., 2021), and regions near TP, like the Yunnan-Guizhou Plateau (Wang et al., 2023). In these regions, the synergistic effects of increased summer SAT and $SW_{\downarrow}$ primarily contribute to the rapid lake warming, and the melting of ice and snow cover can amplify this effect (O'Reilly et al., 2015; Smits et al., 2020). Whereas in TP, $SW_{\downarrow}$ is the main energy source for lake surface budgets but has significantly declined and offset the enhanced $LW_{\downarrow}$, which results in little radiation into lakes and slows down the lakes warming through the feedback of evaporative cooling (Tong et al., 2023; Wang et al., 2018). If $SW_{\downarrow}$ remained zero trends on all TP lakes, that is, compensating the negative trend of $SW_{\downarrow}$ (Figure 8d) on the simulated LSWT trend (Figure 4c), the mean LSWT trend would be 0.44°C decade^{-1} and 56% of lakes would warm faster than air; if $SW_{\downarrow}$ was synergistically enhanced with SAT and opposite to the current trend values, the mean LSWT trend would have been 0.52°C decade^{-1} and up to 72% of lakes would warm faster. Therefore, the weakening $SW_{\downarrow}$ is a key factor explaining the difference between the warming trends of TP lakes and other ice-covered lakes worldwide.

4.3. Uncertainty and Limitations

Given the remote location and harsh environment of TP, reanalysis data from various sources (e.g., ERA5-Land, JRA-55) lack in situ observations from the central and western TP for assimilation, which inevitably introduces errors in our simulations, especially for lakes over western and northern TP (Figure 1). We drive the lake model using JRA-55 instead of ERA5-Land, because ERA5, while performing well in daily variation and climatology, is less effective at capturing the long-term trends in SAT and WS over TP region (H. Liu et al., 2021; Peng et al., 2021; Yao & Li, 2016). This is crucial for attributing lake warming.

Additionally, the heat fluxes from inflows and outflows are unresolved in the WRF-Lake model but important for glacial-fed lakes. It has been reported that inflows from glacial meltwater would cause the cooling of glacial-fed lakes in the context of TP climate warming (Fink et al., 2014; Wan et al., 2018), yet such lake runoff observations are lacking. Furthermore, the present study ignores the temporal variations of lake parameters. For example, the light extinction coefficient allows for dynamic feedback on lake systems based on biochemical processes, and morphological parameters like area and depth can modulate the impacts of the atmosphere on LSWT (Kraemer et al., 2015; Magee & Wu, 2017).

Lake parameters, for example, depth, salinity, and extinction coefficient, are set as constants in the model, which may underestimate the impact of climate change on lake systems (Rose et al., 2016). According to the statistics of 81 lakes in this study (Figure S3 in Supporting Information S1), the simulated LSWT trend is negatively correlated with lake depth ($p = 0.111$) and positively correlated with salinity ($p = 0.072$) and light extinction coefficient ($p = 0.061$). With lake volume and water clarity increasing (Pi et al., 2020; Xu et al., 2022), lake depth and extinction coefficients would decrease, thereby possibly mitigating lake warming by increasing heat capacity and decreasing surface radiation absorption. However, the correlation is not significant statistically, and some studies indicated that LSWT trends are more influenced by geographic factors (e.g., latitude and elevation) and external drivers than by lake morphometry (Pilla et al., 2020; Stefanidis et al., 2022). Overall, further quantitative studies are needed to understand how lake parameters modulate the response of LSWT to climate change.

In this study, we used a different approach than the traditional method to quantify the contributions of atmospheric variables to the LSWT trend. The traditional method estimates contributions by taking the difference in simulated LSWT trends before and after de-trending the target atmospheric forcing variable one-by-one (Huang et al., 2023;

Li et al., 2019, 2023). Its advantages are the simple experimental design and intuitive understanding of the results, but the method neglects the strong interactions between atmospheric forcing variables when de-trending single forcing variable. Our method overcomes this weakness and introduces the absolute sensitivity to quantify the effect of atmospheric forcing on the LSWT in the climatic state, though it requires additional computational expense.

In attribution analysis, the estimated trends tend to be underestimated for colder lakes with larger warming trends (Figure 7c). This might be bias in the calculation of S_a. In Section 2.4.1, $S_a = \frac{\partial \overline{\mathrm{LSWT}}}{\partial \overline{F}}$ is calculated as the slope of perturbation series $\overline{\mathrm{LSWT}}(\overline{F})$, our results show that this series is not strictly linear. For example, the $\overline{\mathrm{LSWT}}(\overline{\mathrm{SAT}})$ demonstrates a decelerated increase, suggesting that at higher $\overline{\mathrm{SAT}}$ levels, $\overline{\mathrm{LSWT}}$ to responses less to equivalent unit changes in $\overline{\mathrm{SAT}}$ Therefore, the calculated S_a–SAT would be smaller than that in current climate state. Similar biases may exist in other S_a–F calculations, which could be amplified by the atmospheric trend $\frac{dF}{dt}$ in Equation 11, resulting in greater underestimation of LSWT trends where $\frac{dF}{dt}$ is larger.

Additionally, the lake system is linearized by Equation 11 in our method and the absolute sensitivity S_{a_i} for F_i is treated as a constant. However, as previously discussed, S_{a_i} should vary with all atmospheric variables F_j (i and j can be equal), that is, $S_{a_i}(t) = S_{a_i}(F_j(t))$, and thus S_{a_i} is also time-varying. For example, decreased SAT or radiation would cause a colder climate, resulting in larger S_{a_i} for the thermodynamic variables. The omitted higher order derivative term may be more important in comparison (Chen et al., 2020). Actually, atmospheric variables and LSWT do not always vary linearly with time, but we only calculate their linear trends. This may affect our results and requires further investigation.

5. Summary

In this study, we use the 1-D WRF-lake model to simulate the LSWT of 81 TP lakes, each with an area ≥50 km^2, during the summers of 1980–2018. Our simulations reasonably reproduce the seasonal cycle and short-term trend patterns of LSWT. The summer LSWT increases with an average of 0.32°C decade^{-1}, which is slightly smaller than the global average rate of lake warming (0.34°C decade^{-1}) during the summers of 1985–2009. The northern TP lakes warm faster than those in the south. Despite most studied lakes being seasonally ice-covered, only 21 (32.1%) of lakes warm faster than the ambient air, differing from other seasonally ice-covered lakes globally. This discrepancy might be due to the widespread weakening of $\mathrm{SW}_\downarrow$ over the TP, which slows down lake warming.

Based on a series of sensitivity experiments, we obtain the absolute sensitivity S_a and relative sensitivity S_r of LSWT to the climatic perturbation of atmospheric forcing variables. On average, the LSWT is most sensitive to $\mathrm{SW}_\downarrow$ and WS, followed by the SAT, $\mathrm{LW}_\downarrow$, and SSH. Spatially, the lakes over the northern TP are more sensitive to the atmospheric thermodynamic variables than those over the southern TP. This is primarily because the lakes located further north, with higher latitude and altitude, experience much colder climates, resulting in lower climatic mean LSWT and larger sensitivities to atmospheric changes.

We estimate the contributions of atmospheric forcing variables to long-term summer LSWT trends using the partial derivative decomposition and ZCA transformation. The air warming and wetting over TP dominate lake warming. In terms of synthesis contribution, air warming contributes 79.3% with increased SAT and $\mathrm{LW}_\downarrow$ accounting for 41.6% and 37.7%, and air wetting, that is, increased SSH contributed 39.0%, followed by the positive contribution (16.8%) of the declined WS. The negative contribution (−35.1%) from the weakened $\mathrm{SW}_\downarrow$ nearly counterbalances the positive impact of $\mathrm{LW}_\downarrow$. The interaction among atmospheric forcing variables accounts for 55.1% of the total contribution, labeled as the cross contribution. Predominantly, the cross contribution stems from SAT and SSH with contributions of 26.8% and 24.8%, while WS, $\mathrm{SW}_\downarrow$, and $\mathrm{LW}_\downarrow$ contribute 10.2%, −14.0%, and 7.3% to the cross contributions, respectively.

Data Availability Statement

These data sets used in this study as follows: the Japanese 55-year Reanalysis (Japan Meteorological Agency, Japan, 2013), https://rda.ucar.edu/datasets/ds628.0/dataaccess/; the latitude, longitude, elevation, average depth of TP lakes (Wang, 2021), https://data.tpdc.ac.cn/en/data/d09ddae6-75c6-431c-a9e4-02e3067e9e1d/; the lake boundary vector data (Zhang, 2019), https://data.tpdc.ac.cn/en/data/98c8fdaa-9451-4a22-b0cf-32f8fd93637e; the

lake salinity data (Zhu, 2021), https://dx.doi.org/10.11888/Hydro.tpdc.271744; the water clarity product (Tao et al., 2021), http://dx.doi.org/10.11888/Hydro.tpdc.271571; the MODIS/Terra MOD11A1 (Wan et al., 2015): https://lpdaac.usgs.gov/products/mod11a1v006/. *Software*—Calculations in this study were finished by the GNU Fortran compiler (GFortran) version 7.5.0, https://gcc.gnu.org/wiki/GFortran-Source. All figures were made by the Python package ProPlot V0.8.0 (Davis, 2021): https://proplot.readthedocs.io/en/latest/index.html.

Acknowledgments
This study is funded by the National Natural Science Foundation of China under Grants 41975081, 42305015, 41975130, CAS "Light of West China" Program (E129030101, Y929641001), the Jiangsu University "Blue Project" outstanding young teachers training object, the Jiangsu Collaborative Innovation Center for Climate Change, the basic research fund of CAMS (2023Y012), and the research project of Jiangsu Meteorological Bureau (KQ202313).

References

Adrian, R., O'Reilly, C. M., Zagarese, H., Baines, S. B., Hessen, D. O., Keller, W., et al. (2009). Lakes as sentinels of climate change. *Limnology & Oceanography*, *54*(6), 2283–2297. https://doi.org/10.4319/lo.2009.54.6_part_2.2283

Anderson, E. J., Stow, C. A., Gronewold, A. D., Mason, L. A., McCormick, M. J., Qian, S. S., et al. (2021). Seasonal overturn and stratification changes drive deep-water warming in one of Earth's largest lakes. *Nature Communications*, *12*(1), 1688. https://doi.org/10.1038/s41467-021-21971-1

Austin, J. A., & Colman, S. M. (2007). Lake superior summer water temperatures are increasing more rapidly than regional air temperatures: A positive ice-albedo feedback. *Geophysical Research Letters*, *34*(6), L06604. https://doi.org/10.1029/2006GL029021

Bell, A. J., & Sejnowski, T. J. (1997). The "independent components" of natural scenes are edge filters. *Vision Research*, *37*(23), 3327–3338. https://doi.org/10.1016/S0042-6989(97)00121-1

Bernus, A., Ottlé, C., & Raoult, N. (2021). Variance based sensitivity analysis of FLake Lake Model for global land surface modeling. *Journal of Geophysical Research: Atmospheres*, *126*(8), e2019JD031928. https://doi.org/10.1029/2019JD031928

Bolton, D. (1980). The computation of equivalent potential temperature. *Monthly Weather Review*, *108*(7), 1046–1053. https://doi.org/10.1175/1520-0493(1980)108<1046:TCOEPT>2.0.CO;2

Bukata, R. P., Jerome, J. H., & Bruton, J. E. (1988). Relationships among Secchi disk depth, beam attenuation coefficient, and irradiance attenuation coefficient for great lakes waters. *Journal of Great Lakes Research*, *14*(3), 347–355. https://doi.org/10.1016/S0380-1330(88)71564-6

Butcher, J. B., Nover, D., Johnson, T. E., & Clark, C. M. (2015). Sensitivity of lake thermal and mixing dynamics to climate change. *Climatic Change*, *129*(1), 295–305. https://doi.org/10.1007/s10584-015-1326-1

Cai, Y., Ke, C.-Q., Li, X., Zhang, G., Duan, Z., & Lee, H. (2019). Variations of Lake ice phenology on the Tibetan plateau from 2001 to 2017 based on MODIS data. *Journal of Geophysical Research: Atmospheres*, *124*(2), 825–843. https://doi.org/10.1029/2018JD028993

Chen, C., Wang, L., Myneni, R. B., & Li, D. (2020). Attribution of land-use/land-cover change induced surface temperature anomaly: How accurate is the first-order Taylor series expansion? *Journal of Geophysical Research: Biogeosciences*, *125*(9), e2020JG005787. https://doi.org/10.1029/2020JG005787

Chen, L., Pryor, S. C., Wang, H., & Zhang, R. (2019). Distribution and variation of the surface sensible heat flux over the central and eastern Tibetan plateau: Comparison of station observations and multireanalysis products. *Journal of Geophysical Research: Atmospheres*, *124*(12), 6191–6206. https://doi.org/10.1029/2018JD030069

Davis, L. L. B. (2021). ProPlot (version 0.8.0) [Software]. *Zenodo*. https://doi.org/10.5281/zenodo.5219856

Davis, P. J. (1975). *Interpolation and approximation*. Courier Corporation.

Fink, G., Schmid, M., Wahl, B., Wolf, T., & Wüest, A. (2014). Heat flux modifications related to climate-induced warming of large European lakes. *Water Resources Research*, *50*(3), 2072–2085. https://doi.org/10.1002/2013WR014448

Fu, G., Shen, Z., Zhang, X., Shi, P., Zhang, Y., & Wu, J. (2011). Estimating air temperature of an alpine meadow on the Northern Tibetan Plateau using MODIS land surface temperature. *Acta Ecologica Sinica*, *31*(1), 8–13. https://doi.org/10.1016/j.chnaes.2010.11.002

Gu, H., Jin, J., Wu, Y., Ek, M. B., & Subin, Z. M. (2015). Calibration and validation of lake surface temperature simulations with the coupled WRF-lake model. *Climatic Change*, *129*(3), 471–483. https://doi.org/10.1007/s10584-013-0978-y

Guo, L., Zheng, H., Wu, Y., Fan, L., Wen, M., Li, J., et al. (2022). An integrated dataset of daily Lake surface water temperature over the Tibetan Plateau. *Earth System Science Data*, *14*(7), 3411–3422. https://doi.org/10.5194/essd-14-3411-2022

Hafner, T. A., & Smith, R. B. (1985). Pressure drag on the European Alps in relation to synoptic events. *Journal of the Atmospheric Sciences*, *42*(6), 562–575. https://doi.org/10.1175/1520-0469(1985)042<0562:PDOTEA>2.0.CO;2

Harada, Y., Kamahori, H., Kobayashi, C., Endo, H., Kobayashi, S., Ota, Y., et al. (2016). The JRA-55 reanalysis: Representation of atmospheric circulation and climate variability. *Journal of the Meteorological Society of Japan. Ser. II*, *94*(3), 269–302. https://doi.org/10.2151/jmsj.2016-015

Henderson-Sellers, B. (1985). New formulation of Eddy diffusion thermocline models. *Applied Mathematical Modelling*, *9*(6), 441–446. https://doi.org/10.1016/0307-904X(85)90110-6

Hostetler, S., & Bartlein, P. (1990). Simulation of lake evaporation with application to modeling lake level variations of Harney-Malheur Lake, Oregon. *Water Resources Research*, *20*(10), 2603–2612. https://doi.org/10.1029/WR026I010P02603

Hsu, S. A. (1988). *Coastal meteorology*. Academic Press Inc.

Huang, A., Lazhu, Wang, J., Dai, Y., Yang, K., Wei, N., et al. (2019). Evaluating and improving the performance of three 1-D lake models in a large deep lake of the central Tibetan plateau. *Journal of Geophysical Research: Atmospheres*, *124*(6), 3143–3167. https://doi.org/10.1029/2018JD029610

Huang, A., Rao, Y. R., & Zhang, W. (2012). On recent trends in atmospheric and Limnological variables in lake Ontario. *Journal of Climate*, *25*(17), 5807–5816. https://doi.org/10.1175/JCLI-D-11-00495.1

Huang, L., Wang, J., Zhu, L., Ju, J., & Daut, G. (2017). The warming of large lakes on the Tibetan plateau: Evidence from a Lake Model simulation of Nam Co, China, during 1979–2012. *Journal of Geophysical Research: Atmospheres*, *122*(24), 13095–13107. https://doi.org/10.1002/2017JD027379

Huang, L., Wang, X., Sang, Y., Tang, S., Jin, L., Yang, H., et al. (2021). Optimizing Lake surface water temperature simulations over large lakes in China with FLake model. *Earth and Space Science*, *8*(8), e2021EA001737. https://doi.org/10.1029/2021EA001737

Huang, L., Wang, X., Yan, Y., Jin, L., Yang, K., Chen, A., et al. (2023). Attribution of Lake Surface water temperature change in large lakes across China over past four decades. *Journal of Geophysical Research: Atmospheres*, *128*(21), e2022JD038465. https://doi.org/10.1029/2022JD038465

Japan Meteorological Agency, Japan. (2013). JRA-55: Japanese 55-year reanalysis, daily 3-hourly and 6-hourly data [Dataset]. *Research Data Archive at the National Center for Atmospheric Research, Computational and Information Systems Laboratory*. https://doi.org/10.5065/D6HH6H41

Kessy, A., Lewin, A., & Strimmer, K. (2018). Optimal whitening and decorrelation. *The American Statistician*, *72*(4), 309–314. https://doi.org/10.1080/00031305.2016.1277159

Kirillin, G., Wen, L., & Shatwell, T. (2017). Seasonal thermal regime and climatic trends in lakes of the Tibetan highlands. *Hydrology and Earth System Sciences*, *21*(4), 1895–1909. https://doi.org/10.5194/hess-21-1895-2017

Kobayashi, S., Ota, Y., Harada, Y., Ebita, A., Moriya, M., Onoda, H., et al. (2015). The JRA-55 reanalysis: General specifications and basic characteristics. *Journal of the Meteorological Society of Japan. Ser. II*, *93*(1), 5–48. https://doi.org/10.2151/jmsj.2015-001

Kraemer, B. M., Anneville, O., Chandra, S., Dix, M., Kuusisto, E., Livingstone, D. M., et al. (2015). Morphometry and average temperature affect lake stratification responses to climate change. *Geophysical Research Letters*, *42*(12), 4981–4988. https://doi.org/10.1002/2015GL064097

Kuang, X., & Jiao, J. J. (2016). Review on climate change on the Tibetan Plateau during the last half century. *Journal of Geophysical Research: Atmospheres*, *121*(8), 3979–4007. https://doi.org/10.1002/2015JD024728

Lang, J., Ma, Y., Li, Z., & Su, D. (2021). The impact of climate warming on Lake Surface heat exchange and ice phenology of different types of lakes on the Tibetan plateau. *Water*, *13*(5), 634. https://doi.org/10.3390/w13050634

Layden, A., MacCallum, S. N., & Merchant, C. J. (2016). Determining Lake surface water temperatures worldwide using a tuned one-dimensional lake model (FLake, v1). *Geoscientific Model Development*, *9*(6), 2167–2189. https://doi.org/10.5194/gmd-9-2167-2016

Lazhu, Yang, K., Qin, J., Hou, J., Lei, Y., Wang, J., et al. (2022). A strict validation of MODIS Lake Surface water temperature on the Tibetan plateau. *Remote Sensing*, *14*(21), 5454. https://doi.org/10.3390/rs14215454

Lazhu, Yang, K., Wang, J., Lei, Y., Chen, Y., Zhu, L., & Qin, J. (2016). Quantifying evaporation and its decadal change for Lake Nam Co, central Tibetan Plateau. *Journal of Geophysical Research: Atmospheres*, *121*(13), 7578–7591. https://doi.org/10.1002/2015JD024523

Li, H., Sun, D., Yu, Y., Wang, H., Liu, Y., Liu, Q., et al. (2014). Evaluation of the VIIRS and MODIS LST products in an arid area of Northwest China. *Remote Sensing of Environment*, *142*, 111–121. https://doi.org/10.1016/j.rse.2013.11.014

Li, J., Sun, J., Wang, R., Cui, T., & Tong, Y. (2023). Warming of surface water in the large and shallow lakes across the Yangtze River Basin, China, and its driver analysis. *Environmental Science and Pollution Research*, *30*(8), 20121–20132. https://doi.org/10.1007/s11356-022-23608-2

Li, X., Peng, S., Deng, X., Su, M., & Zeng, H. (2019). Attribution of Lake warming in four shallow lakes in the middle and lower Yangtze river basin. *Environmental Science & Technology*, *53*(21), 12548–12555. https://doi.org/10.1021/acs.est.9b03098

Liu, B., Wan, W., Xie, H., Li, H., Zhu, S., Zhang, G., et al. (2019). A long-term dataset of Lake surface water temperature over the Tibetan Plateau derived from AVHRR 1981–2015. *Scientific Data*, *6*(1), 48. https://doi.org/10.1038/s41597-019-0040-7

Liu, C., Zhu, L., Wang, J., Ju, J., Ma, Q., Qiao, B., et al. (2021a). In situ water quality investigation of the lakes on the Tibetan Plateau. *Science Bulletin*, *66*(17), 1727–1730. https://doi.org/10.1016/j.scib.2021.04.024

Liu, H., Dong, L., Yan, R., Zhang, X., Guo, C., Liang, S., et al. (2021b). Evaluation of near-surface wind speed climatology and long-term trend over China's mainland region based on ERA5 reanalysis (in Chinese). *Climatic and Environmental Research*, *26*(3), 299–311. https://doi.org/10.3878/j.issn.1006-9585.2021.20101

Magee, M. R., & Wu, C. H. (2017). Response of water temperatures and stratification to changing climate in three lakes with different morphometry. *Hydrology and Earth System Sciences*, *21*(12), 6253–6274. https://doi.org/10.5194/hess-21-6253-2017

Mironov, D., Heise, E., Kourzeneva, E., Ritter, B., Schneider, N., & Terzhevik, A. (2010). Implementation of the lake parameterisation scheme FLake into the numerical weather prediction model COSMO. *Boreal Environment Research*, *15*, 218–230.

Murray, F. W. (1967). On the computation of saturation vapor pressure. *Journal of Applied Meteorology and Climatology*, *6*(1), 203–204. https://doi.org/10.1175/1520-0450(1967)006<0203:OTCOSV>2.0.CO;2

O'Reilly, C. M., Sharma, S., Gray, D. K., Hampton, S. E., Read, J. S., Rowley, R. J., et al. (2015). Rapid and highly variable warming of Lake surface waters around the globe. *Geophysical Research Letters*, *42*(24), 10773–10781. https://doi.org/10.1002/2015GL066235

Peng, X., Frauenfeld, O. W., Jin, H., Du, R., Qiao, L., Zhao, Y., et al. (2021). Assessment of temperature changes on the Tibetan plateau during 1980–2018. *Earth and Space Science*, *8*(4), e2020EA001609. https://doi.org/10.1029/2020EA001609

Pi, X., Feng, L., Li, W., Zhao, D., Kuang, X., & Li, J. (2020). Water clarity changes in 64 large alpine lakes on the Tibetan Plateau and the potential responses to lake expansion. *ISPRS Journal of Photogrammetry and Remote Sensing*, *170*, 192–204. https://doi.org/10.1016/j.isprsjprs.2020.10.014

Piccolroaz, S., Toffolon, M., & Majone, B. (2013). A simple lumped model to convert air temperature into surface water temperature in lakes. *Hydrology and Earth System Sciences*, *17*(8), 3323–3338. https://doi.org/10.5194/hess-17-3323-2013

Pilla, R. M., Williamson, C. E., Adamovich, B. V., Adrian, R., Anneville, O., Chandra, S., et al. (2020). Deeper waters are changing less consistently than surface waters in a global analysis of 102 lakes. *Scientific Reports*, *10*(1), 20514. https://doi.org/10.1038/s41598-020-76873-x

Qiu, J. (2008). China: The third pole. *Nature News*, *454*(7203), 393–396. https://doi.org/10.1038/454393a

Quan, J., Chen, Y., Zhan, W., Wang, J., Voogt, J., & Wang, M. (2014). Multi-temporal trajectory of the urban heat island centroid in Beijing, China based on a Gaussian volume model. *Remote Sensing of Environment*, *149*, 33–46. https://doi.org/10.1016/j.rse.2014.03.037

Roderick, M. L., Rotstayn, L. D., Farquhar, G. D., & Hobbins, M. T. (2007). On the attribution of changing pan evaporation. *Geophysical Research Letters*, *34*(17), L7403. https://doi.org/10.1029/2007GL031166

Rose, K. C., Winslow, L. A., Read, J. S., & Hansen, G. J. A. (2016). Climate-induced warming of Lakes can be either amplified or suppressed by trends in water clarity. *Limnology and Oceanography Letters*, *1*(1), 44–53. https://doi.org/10.1002/lol2.10027

Ruckstuhl, C., Philipona, R., Morland, J., & Ohmura, A. (2007). Observed relationship between surface specific humidity, integrated water vapor, and longwave downward radiation at different altitudes. *Journal of Geophysical Research*, *112*(D3). https://doi.org/10.1029/2006JD007850

Schmid, M., Hunziker, S., & Wüest, A. (2014). Lake surface temperatures in a changing climate: A global sensitivity analysis. *Climatic Change*, *124*(1), 301–315. https://doi.org/10.1007/s10584-014-1087-2

Schmid, M., & Köster, O. (2016). Excess warming of a Central European lake driven by solar brightening. *Water Resources Research*, *52*(10), 8103–8116. https://doi.org/10.1002/2016WR018651

Schneider, P., & Hook, S. J. (2010). Space observations of inland water bodies show rapid surface warming since 1985. *Geophysical Research Letters*, *37*(22), L22405. https://doi.org/10.1029/2010GL045059

Shi, Y., Huang, A., Ma, W., Wen, L., Zhu, L., Yang, X., et al. (2022). Drivers of warming in lake Nam Co on Tibetan plateau over the past 40 years. *Journal of Geophysical Research: Atmospheres*, *127*(16), e2021JD036320. https://doi.org/10.1029/2021JD036320

Shinohara, R., Tanaka, Y., Kanno, A., & Matsushige, K. (2021). Relative impacts of increases of solar radiation and air temperature on the temperature of surface water in a shallow, eutrophic lake. *Hydrology Research*, *52*(4), 916–926. https://doi.org/10.2166/nh.2021.148

Smits, A. P., MacIntyre, S., & Sadro, S. (2020). Snowpack determines relative importance of climate factors driving summer lake warming. *Limnology and Oceanography Letters*, *5*(3), 271–279. https://doi.org/10.1002/lol2.10147

Stefanidis, K., Varlas, G., Papaioannou, G., Papadopoulos, A., & Dimitriou, E. (2022). Trends of lake temperature, mixing depth and ice cover thickness of European lakes during the last four decades. *Science of The Total Environment*, *830*, 154709. https://doi.org/10.1016/j.scitotenv.2022.154709

Stetler, J. T., Girdner, S., Mack, J., Winslow, L. A., Leach, T. H., & Rose, K. C. (2021). Atmospheric stilling and warming air temperatures drive long-term changes in lake stratification in a large oligotrophic lake. *Limnology & Oceanography*, *66*(3), 954–964. https://doi.org/10.1002/lno.11654

Su, D., Hu, X., Wen, L., Lyu, S., Gao, X., Zhao, L., et al. (2019). Numerical study on the response of the largest lake in China to climate change. *Hydrology and Earth System Sciences*, *23*(4), 2093–2109. https://doi.org/10.5194/hess-23-2093-2019

Subin, Z. M., Riley, W. J., & Mironov, D. (2012). An improved lake model for climate simulations: Model structure, evaluation, and sensitivity analyses in CESM1. *Journal of Advances in Modeling Earth Systems*, *4*(1), M02001. https://doi.org/10.1029/2011MS000072

Tao, H., Song, K., Liu, G., Wang, Q., & Wen, Z. (2021). Water clarity annual dynamics dataset across China (1990–2018) [Dataset]. *National Tibetan Plateau Data Center*. https://doi.org/10.11888/Hydro.tpdc.271571

Tao, H., Song, K., Liu, G., Wang, Q., Wen, Z., Jacinthe, P.-A., et al. (2022). A Landsat-derived annual inland water clarity dataset of China between 1984 and 2018. *Earth System Science Data*, *14*(1), 79–94. https://doi.org/10.5194/essd-14-79-2022

Tong, Y., Feng, L., Wang, X., Pi, X., Xu, W., & Woolway, R. I. (2023). Global lakes are warming slower than surface air temperature due to accelerated evaporation. *Nature Water*, *1*(11), 929–940. https://doi.org/10.1038/s44221-023-00148-8

Wan, W., Zhao, L., Xie, H., Liu, B., Li, H., Cui, Y., et al. (2018). Lake surface water temperature change over the Tibetan plateau from 2001 to 2015: A sensitive indicator of the warming climate. *Geophysical Research Letters*, *45*(20), 11177–11186. https://doi.org/10.1029/2018GL078601

Wan, Z., Hook, S., & Hulley, G. (2015). MOD11A1 MODIS/terra land surface temperature/emissivity daily L3 global 1km SIN grid V006 [Dataset]. *NASA EOSDIS Land Processes DAAC*. https://doi.org/10.5067/MODIS/MOD11A1.006

Wang, W., Lee, X., Xiao, W., Liu, S., Schultz, N., Wang, Y., et al. (2018). Global lake evaporation accelerated by changes in surface energy allocation in a warmer climate. *Nature Geoscience*, *11*(6), 410–414. https://doi.org/10.1038/s41561-018-0114-8

Wang, X. (2021). Long time series data set of north temperate lake ice cover occurrence values (1985–2020) [Dataset]. *National Tibetan Plateau Data Center*. https://doi.org/10.11888/Hydro.tpdc.271744

Wang, X., Feng, L., Gibson, L., Qi, W., Liu, J., Zheng, Y., et al. (2021). High-resolution mapping of ice cover changes in over 33,000 lakes across the North temperate zone. *Geophysical Research Letters*, *48*(18). https://doi.org/10.1029/2021GL095614

Wang, X., Shi, K., Zhang, Y., Qin, B., Zhang, Y., Wang, W., et al. (2023). Climate change drives rapid warming and increasing heatwaves of lakes. *Science Bulletin*, *68*(14), 1574–1584. https://doi.org/10.1016/j.scib.2023.06.028

Wen, L., Lyu, S., Kirillin, G., Li, Z., & Zhao, L. (2016). Air–lake boundary layer and performance of a simple lake parameterization scheme over the Tibetan highlands. *Tellus A: Dynamic Meteorology and Oceanography*, *68*(1), 31091. https://doi.org/10.3402/tellusa.v68.31091

Wen, L., Nagabhatla, N., Zhao, L., Li, Z., & Chen, S. (2015). Impacts of salinity parameterizations on temperature simulation over and in a hypersaline lake. *Chinese Journal of Oceanology and Limnology*, *33*(3), 790–801. https://doi.org/10.1007/s00343-015-4153-3

Woolway, R. I., Kraemer, B. M., Lenters, J. D., Merchant, C. J., O'Reilly, C. M., & Sharma, S. (2020). Global lake responses to climate change. *Nature Reviews Earth & Environment*, *1*(8), 388–403. https://doi.org/10.1038/s43017-020-0067-5

Woolway, R. I., & Merchant, C. J. (2017). Amplified surface temperature response of cold, deep lakes to inter-annual air temperature variability. *Scientific Reports*, *7*(1), 4130. https://doi.org/10.1038/s41598-017-04058-0

Woolway, R. I., Merchant, C. J., Hoek, J. V. D., Azorin-Molina, C., Nõges, P., Laas, A., et al. (2019). Northern hemisphere atmospheric stilling accelerates lake thermal responses to a warming world. *Geophysical Research Letters*, *46*(21), 11983–11992. https://doi.org/10.1029/2019GL082752

Wu, Y., Huang, A., Lazhu, Yang, X., Qiu, B., Wen, L., et al. (2020). Improvements of the coupled WRF-Lake model over lake Nam Co, central Tibetan plateau. *Climate Dynamics*, *55*(9–10), 2703–2724. https://doi.org/10.1007/s00382-020-05402-3

Wu, Y., Huang, A., Li, X., Wen, L., Li, J., & Li, J. (2024). Thermal response of large seasonally ice-covered lakes over Tibetan plateau to climate change. *Journal of Geophysical Research: Atmospheres*, *129*(8), e2023JD039935. https://doi.org/10.1029/2023JD039935

Xu, F., Zhang, G., Yi, S., & Chen, W. (2022). Seasonal trends and cycles of lake-level variations over the Tibetan Plateau using multi-sensor altimetry data. *Journal of Hydrology*, *604*, 127251. https://doi.org/10.1016/j.jhydrol.2021.127251

Xu, J., Tian, R., & Feng, S. (2021). Comparison of atmospheric vertical motion over China in ERA-interim, JRA-55, and NCEP/NCAR reanalysis datasets. *Asia-Pacific Journal of Atmospheric Sciences*, *57*(4), 773–786. https://doi.org/10.1007/s13143-021-00226-5

Xu, X., Lu, C., Shi, X., & Gao, S. (2008). World water tower: An atmospheric perspective. *Geophysical Research Letters*, *35*(20), L20815. https://doi.org/10.1029/2008GL035867

Yan, Y., Liu, X., Wen, Y., & Ou, J. (2019). Quantitative analysis of the contributions of climatic and human factors to grassland productivity in Northern China. *Ecological Indicators*, *103*, 542–553. https://doi.org/10.1016/j.ecolind.2019.04.020

Yang, K., Ding, B., Qin, J., Tang, W., Lu, N., & Lin, C. (2012). Can aerosol loading explain the solar dimming over the Tibetan Plateau? *Geophysical Research Letters*, *39*(20), L20710. https://doi.org/10.1029/2012GL053733

Yang, K., Wu, H., Qin, J., Lin, C., Tang, W., & Chen, Y. (2014). Recent climate changes over the Tibetan Plateau and their impacts on energy and water cycle: A review. *Global and Planetary Change*, *112*, 79–91. https://doi.org/10.1016/j.gloplacha.2013.12.001

Yao, H., & Li, D. (2016). The interannual variation of wind speed in the Tibetan Plateau in spring and its response to global warming during 1971–2012 (in Chinese). *Acta Meteorologica Sinica*, *74*(1), 60–75.

Yuan, M., Leirvik, T., & Wild, M. (2021). Global trends in downward surface solar radiation from spatial interpolated ground observations during 1961–2019. *Journal of Climate*, *34*(23), 9501–9521. https://doi.org/10.1175/JCLI-D-21-0165.1

Yusufova, V. D., Pepinov, R. I., Nikolaev, V. A., & Guseinov, G. M. (1975). Thermal conductivity of aqueous solutions of NaCl. *Journal of Engineering Physics*, *29*(4), 1225–1229. https://doi.org/10.1007/BF00867119

Zhang, G. (2019). The lakes larger than 1k㎡ in Tibetan Plateau (V1.0) (1970s, 1990, 2000, 2010) [Dataset]. *National Tibetan Plateau Data Center*. https://doi.org/10.11888/Lake.tpe.249481.file

Zhang, G., Luo, W., Chen, W., & Zheng, G. (2019). A robust but variable lake expansion on the Tibetan Plateau. *Science Bulletin*, *64*(18), 1306–1309. https://doi.org/10.1016/j.scib.2019.07.018

Zhang, G., Yao, T., Xie, H., Qin, J., Ye, Q., Dai, Y., & Guo, R. (2014). Estimating surface temperature changes of lakes in the Tibetan Plateau using MODIS LST data. *Journal of Geophysical Research: Atmospheres*, *119*(14), 8552–8567. https://doi.org/10.1002/2014JD021615

Zhang, H., Immerzeel, W. W., Zhang, F., de Kok, R. J., Gorrie, S. J., & Ye, M. (2021). Creating 1-km long-term (1980–2014) daily average air temperatures over the Tibetan Plateau by integrating eight types of reanalysis and land data assimilation products downscaled with MODIS-estimated temperature lapse rates based on machine learning. *International Journal of Applied Earth Observation and Geoinformation*, *97*, 102295. https://doi.org/10.1016/j.jag.2021.102295

Zhou, J., Leavitt, P. R., Rose, K. C., Wang, X., Zhang, Y., Shi, K., & Qin, B. (2023). Controls of thermal response of temperate lakes to atmospheric warming. *Nature Communications*, *14*(1), 6503. https://doi.org/10.1038/s41467-023-42262-x

Zhu, L. (2021). In situ water quality parameters of the lakes on the Tibetan Plateau (2009-2020) [Dataset]. *National Tibetan Plateau Data Center*. https://doi.org/10.11888/Geogra.tpdc.271450